INTERNATIONAL JOURNAL OF CLIMATOLOGY
Int. J. Climatol. **26**: 1283–1314 (2006)
Published online 6 April 2006 in Wiley InterScience (www.interscience.wiley.com). DOI: 10.1002/joc.1308

IMPACT OF GLOBAL WARMING ON ENSO VARIABILITY USING THE COUPLED GISS GCM/ZC MODEL

TIMOTHY EICHLER,[a,*] DAVID RIND[b] and STEPHEN ZEBIAK[c]

[a] *Research Scientist, Goddard Institute for Space Studies, 2880 Broadway, NY 10025, New York*
[b] *Senior Research Scientist, Goddard Institute for Space Studies, 2880 Broadway, NY 10025, New York*
[c] *Director, Modeling and Prediction Research, International Research for Climate Prediction, Lamont-Doherty Earth Observatory, Palisades, NY 10964, New York*

Received 15 October 2004
Revised 20 August 2005
Accepted 22 November 2005

ABSTRACT

This study uses a hybrid coupled model (referred to as the general-circulation model (GCM)/Zebiak/Cane (ZC) model), which consists of the Goddard Institute for Space Studies' (GISS) Atmospheric general-circulation model (AGCM) coupled to the oceanic component of the ZC intermediate model to assess the impact of global warming on El Niño behavior, with and without the influence of heat introduced from the subtropical Pacific (via subtropical cell (STC) pathway). The baseline GCM/ZC model produces El Niño variability with a two year periodicity and an amplitude of approximately half the magnitude of observed El Niño. The GCM/ZC model also produces an appropriate atmospheric global response to El Niño/southern oscillation (ENSO) as shown by composites of 500 hPa heights, sea-level pressure (SLP), 200 hPa wind, and precipitation during El Niño and La Niña periods. To evaluate the importance of global warming on ENSO variability, $2\times$ CO_2 and $4\times$ CO_2 transient simulations were done increasing the atmospheric CO_2 one percent per year, then extending the runs for an additional 70 years to obtain equilibrium climates for each run. An additional set of global-warming simulations was run after including a STC parameterization generated by computing 5-year running means of the sea-surface temperature (SST) difference between a transient run and the $1\times$ CO_2 GCM/ZC run at the anticipated subduction zones (160–130 °W, 20–40 °N and 20–44 °S, 160–130 °W) and adding it to the base of the equatorial mixed-layer of the ZC model with a time lag of 15 years. This effectively alters the vertical temperature gradient of the ZC model, which affects SST via upwelling.

Two features of the GCM/ZC response to global warming are emphasized. Firstly, the inclusion of the STC results in a major redistribution of heat across the equatorial Pacific, leading to an El Niño-like response in the final equilibrium solution with less variability about the mean. The global warming aspect due to the El Niño-like response results in a positive feedback on global warming, which causes a higher global surface-air temperature (SAT) than identical transient simulations without inclusion of the STC. Secondly, including the STC effect produces a far greater magnitude of global ENSO-like impact because of the reduction of, or even the reversal of, the equatorial Pacific longitudinal SST gradient. The implications of such an extreme climate scenario are discussed. Copyright © 2006 Royal Meteorological Society.

KEY WORDS: El Niño; STC; teleconnections; dynamical thermostat; upwelling; global warming; SST; equilibrium climate

1. INTRODUCTION

Owing to its impact on the global circulation, an important aspect of understanding present and future climate change is the ability of ocean/atmosphere climate models to simulate the El Niño/southern oscillation (ENSO). Early work in this area was summarized by Neelin *et al*. (1992), who described 17 coupled models from various institutions. He found that many of the models contained weak interannual variability because of insufficient coupling strength from an overly strong cold tongue, weak wind-stress response to sea-surface temperature (SST), and flux correction that acted as a damping term. More recent ENSO modeling attempts

* Correspondence to: Dr. Timothy Eichler, NOAA/OAR, 1315 East–West Highway, Silver Spring, MD 20910, USA;
e-mail: tim.eichler@noaa.gov

have also shown a tendency toward weaker than normal ENSO. Falling into this category are the modeling studies of Knutson *et al*. (1997), Tett (1995), Timmerman *et al*. (1999), and Meehl and Arblaster (1998). All of these studies imply that the insufficient ENSO amplitude is because of coarse model resolution. However, model simulations of ENSO are showing progress. For example, Bacher *et al*. (1998) found an ENSO of comparable magnitude to the observed one, though their signal was more frequent than that of the observed (a period of 28 months for their model *vs* 4 years for the observed). Although many of the models failed to simulate ENSO accurately, they did capture many of the basic physical mechanisms thought to govern the real ENSO and so were also used for greenhouse warming studies.

Several of the coupled models used in global-warming studies have contrasting ideas on the physical mechanisms that relate greenhouse warming to ENSO strength/frequency. For example, Clement *et al*. (1996) presented a 'thermostat' theory, in which an increase in vertical heat flux into the equatorial Pacific would increase the temperature of the western Pacific relative to the eastern Pacific because the increase in heat flux in the eastern Pacific is partially offset by upwelling. Thus, the zonal temperature gradient would be increased, producing a stronger Walker Circulation, which would cause stronger surface equatorial Easterlies resulting in 'La Niña' conditions across the Pacific. Clement *et al*. (1996) confirmed this effect by imposing a surface forcing of ± 40 W m^{-2} in the model developed by Zebiak and Cane (1987) (ZC model) and noting that the effect on the ocean's surface was opposite to the forcing used. Similar results were generated by Seager and Murtugudde (1997) who used an ocean model described in Murtugudde *et al*. (1996) coupled to an atmospheric mixed-layer model developed by Seager *et al*. (1995). They ran their model for 35 years using climatological forcing, then added a forcing of $+10$ W m^{-2} into the ocean mixed-layer and integrated the model for an additional 70 years. By the end of 70 years, the east–west temperature gradient had increased by 0.6 °C because of the thermostat mechanism in which the heating in the east was partially offset by coastal upwelling. Although the above arguments may suggest that greenhouse warming leads to increased equatorial SST gradients, Murtugudde *et al*. (1996) point out that their model (along with the other modeling studies described above) lacks some crucial ocean dynamics; namely, that of the subtropical cell (STC), in which heat from the surface water at mid and high latitudes is transported via subduction and convection to the deeper ocean, causing a reduction of vertical stability leading to an increase in temperature of the mixed-layer water and a reduction of the equatorial SST gradient. This mechanism is suggested by Gu and Philander (1997), Lu and McCreary (1995), Liu (1994), and McCreary and Lu (1994). Changes in the STC would lead to the upwelling of warm water in the eastern Pacific from warmer surface subtropical water, thus overwhelming the dynamical thermostat. Other modeling studies that are used to study the interaction between global warming and the equatorial Pacific SST gradient include Liu (1998) who used a box model and found that the equatorial Pacific SST changes went through two distinct phases. The first was referred to as the 'surface adjustment phase' and was characterized by weak warming in the cold tongue, strong warming in the warm pool, and the strongest warming in the extratropics. This had the effect of increasing the longitudinal temperature gradient in a manner similar to Seager and Murtugudde (1997) and Clement *et al*. (1996). In the second phase, labeled the 'thermocline adjustment phase', the SST evolved toward an equilibrium dependent on the nonlinear interaction with the extratropics. This caused a decrease in longitudinal temperature gradient across the equatorial Pacific.

Although intriguing, two points should be made about the results of Liu (1998). Firstly, as pointed out in that study, observational analysis (Cane *et al*., 1997; Latif *et al*., 1997; Kaplan *et al*., 1998) indicates an increased SST contrast in the central equatorial Pacific. Although Liu (1998) states that the observations may contain large errors, Liu (1998) also states that it is quite possible that coupled general-circulation models (GCMs) lack some key physics. Similarly, Meehl and Washington (1996) used the observed Pacific SST data from the United Kingdom Meteorological Office (UKMO) analysis and found a reduction and not an enhancement of SST gradient, more in line with model results. Secondly, the model used by Liu (1998) is a simple box model and therefore does not contain the atmospheric processes pertaining to studying CO_2 effects.

A question raised by the STC mechanism described by Gu and Philander (1997) is whether the temperature anomalies subducted in the subtropical Pacific can reach the equatorial zone before being dissipated. As described in McPhaden and Zhang (2002), several modeling studies show that the temperature anomalies can

be strongly dissipated, dispersed via planetary-scale ocean waves, or be disrupted by low-latitude changes in surface winds (Schneider *et al*., 1999; Liu and Shin (1999), Nonaka *et al*. (2000)). Kleeman *et al*. (1999) used an intermediate coupled model to demonstrate an alternative mechanism for altering the STC by which the speed of transport in the surface component is changed; as in the Gu and Philander (1997) scheme, the transport of water with constant properties at faster or slower rates toward the equator has significant implications for equatorial upwelling and hence, ENSO variability. Unlike the Gu and Philander (1997) mechanism, changes are most prominent in the upper branch portion of the STC, instead of being induced by temperature changes in the lower branch of the STC, caused by midlatitude changes in surface heat-flux anomalies. Finally, a third mechanism points to the atmosphere being solely responsible for ENSO decadal variability due to the wind-stress anomalies generated in the midlatitudes extending into the tropics (Barnett *et al*., 1999).

Observational evidence using tritium as a tracer supports the idea that a pathway exists for North Pacific waters to reach the equator (Fine *et al*., 1987). Other studies have suggested that additional mechanisms such as the Mindanao current (Liu and Huang, 1998) contribute maximum to the central Pacific tritium. Lee and Fukumori (2003) used a near-global ocean GCM in combination with satellite observations and data assimilation to deduce that interior exchange in the North Pacific is more important to decadal variability in the tropical Pacific than the Mindanao current. Lee and Fukumori (2003) also found that the interior pycnocline flow into the tropics was weaker in the 1990s relative to the 1980s; this is supported by McPhaden and Zhang (2002) who found a slowing down of the overturning circulation since the 1970s. Because a slowing of the overturning circulation is capable of altering upwelling in the eastern equatorial Pacific, this has implications for the impact of global warming on ENSO variability and the equatorial SST gradient.

Other modeling studies have indicated that local effects may impact ENSO variability. For example, Timmerman *et al*. (1999) used the climate model developed at the Max Planck Institute and ran a 300-year scenario with fixed present-day concentrations of CO_2 and compared it with a 300-year scenario in which the model was forced by observed CO_2 levels from 1860–1990 according to IPCC scenario IS92a (1990–2100). Collins (2000a) ran the Hadley Center coupled model (HadCM2) finding little change in ENSO variability until $4 \times CO_2$ concentrations relative to preindustrial times was achieved; at which time a 20% increase in amplitude of ENSO events, as well as frequency doubling relative to present climate were noted. However, in a follow-up paper, Collins (2000b) ran a different version of the Hadley Center model (HadCM3) to $4 \times CO_2$ levels and found little change in ENSO variability relative to current climate. Collins (2000b) attributed the result to differences in the mean meridional temperature gradient on either side of the equator because of differences in the physical parameterizations of HADCM3 relative to HADCM2. Timmerman *et al*. (1999) found increased frequency of ENSO in the CO_2 run model relative to control and also stronger La Niña events in response to increased CO_2 levels. Timmerman *et al*. (1999) and Collins (2000a) indicated that a tendency toward more extreme events in response to increased greenhouse gas may have been because of a strengthened thermocline in the eastern equatorial Pacific resulting in an increased sensitivity to wind stress in that region.

Finally, some studies suggest that evaporative feedback in the equatorial Pacific may be the dominant mechanism in controlling global-warming induced ENSO variability; this implies that as SST warms, the nonlinear relationship with evaporation via the Clausius–Clapeyron relationship would act as a constraint on increased SST. Knutson and Manabe (1995) ascribed the above mechanism as being responsible for reducing the longitudinal temperature gradient in their coupled model's response to increased CO_2. Similar results were also obtained by Tett (1995), Knutson *et al*. (1997), Meehl and Washington (1986, 1989, 1996), Oglesby and Saltzman (1992), and Washington and Meehl (1993). Interestingly, Meehl and Washington (1996) also point out that SST warming observed in the equatorial Pacific during the 1980s was nonuniform, with warming in the western Pacific being half that of the warming in the eastern Pacific (0.15 °C *vs* 0.35 °C respectively). In contrast, Meehl *et al*. (2000) found that the National Center for Atmospheric Research (NCAR) climate system model (CSM) produced little change in the equatorial SST gradient. Meehl *et al*. (2000) attributed this to negative differences in the net-cloud forcing in the eastern equatorial Pacific. Further observational and modeling studies are needed to better understand the potential impacts of global warming on the longitudinal Pacific SST gradient.

Applications for the coupled ocean/atmosphere models related to ENSO include ENSO forecasting and studying the effects of climate change on ENSO (and vice versa). Some success has been met for the former as first shown by Cane *et al*. (1986) and reviewed by Latif *et al*. (1998). Studies of ENSO and global climate using comprehensive coupled models are difficult, because these models are prone to climate drift and are expensive to run. On the other hand, performing climate change experiments on simplified models such as the Zebiak/Cane (ZC) model are limited for two reasons; firstly, it is a sector model that cannot be used to study global climate and, secondly, many of the processes and feedbacks thought to be important to global change are neglected.

This study bypasses these limitations by coupling the Zebiak/Cane ocean model to the Goddard Institute for Space Studies (GISS) atmospheric general-circulation model (AGCM) containing a q-flux ocean (i.e. an ocean model in which SST is allowed to change because of changes in sensible and latent heat and short and long-wave radiation, referred to in this study as the AGCMq). The final product is an AGCMq coupled to an ocean sector model of the tropical Pacific with the potential to generate ENSO because of the inclusion of a surface-ocean dynamical heating term supplied by the ZC model (described in Section 2).

The coupled model (referred to as the GCM/ZC model) consists of two components. The first is the GISS AGCM, which is a grid-point model containing a resolution of 4° latitude by 5° longitude, with nine vertical layers as described in Hansen *et al*. (1988). It is coupled, in the version used here, to a 'q-flux' ocean model, which is a nondynamic 'slab' model containing a variable depth mixed-layer to a maximum of 250 m, and diffusion below the bottom of this layer, and specified heat transports (hereafter referred to as the AGCMq model). The GISS AGCMq also incorporates an improved boundary layer scheme described in Hartke and Rind (1997), which plays a key role in generating realistic wind-stress forcing. The second component of the coupled model is the ocean component of the ENSO model developed by Zebiak and Cane (1987) (ZC model), whose domain extends from 124 °E to 80 °W and from 29 °S to 29 °N. The ZC model is an anomaly model, with the version used for coupling only allowing SSTs to change because of imposed external wind-stress anomalies, which is a key element missing from the AGCMq.

This study can be broadly divided into two parts. The first part outlines the development of the GCM/ZC model, as well as the ENSO simulating capability of a control version of the model run for fifty years with present-day concentrations of CO_2. Included is a discussion of the GCM's global atmospheric response to the imposed ENSO variability. The second part analyzes the impact of increased atmospheric CO_2 concentrations on the coupled model's ENSO variability. Because the temperature of water upwelled in the eastern Pacific plays a crucial role in determining the final ENSO state's response to global warming, a crude representation of the STC is introduced into some of the simulations so that the importance of ocean dynamics to the final ENSO state can be assessed.

Because the mechanism(s) by which heat is added to the equatorial mixed-layer via the STC is beyond the capability of the GCM/ZC model, it is not as physically complete as the current generation of fully coupled ocean/atmosphere GCMs. However, it does allow for the testing of how changes to the amount of heat transport via the STC can impact ENSO variability and hence, global climate. Since it is unclear how much heat is transported from the STC in response to increased atmospheric greenhouse gas concentrations, the greenhouse gas experiments that include the STC make the assumption that all heat resulting from increases in SST in the subtropical Pacific eventually reaches the base of the equatorial mixed-layer. Although this is an unlikely scenario, it does allow for clearly delineating the physical changes to the global climate system if the STC is altered. The results from this set of experiments should therefore be regarded as a sensitivity study regarding the potential impacts of increased atmospheric greenhouse gas concentrations on ENSO variability. Clearly, continued improvements in fully coupled ocean/atmosphere GCMs will help clarify the physical mechanisms for the transport of heat via the STC, resulting in a more accurate assessment of its impact on the vertical temperature structure of the equatorial Pacific.

With regard to the detailed structure of this manuscript, justification for the development of the coupled system is given in Section 2. Section 3 describes the coupling procedure used for constructing the GCM/ZC model. Sections 4 and 5 detail the ENSO capability and the global response, respectively, for a 50-year simulation of the GCM/ZC model. Section 6 describes the procedure for producing the various global-warming simulations that lead to a discussion of how global warming impacts ENSO variability, given in

Section 7. Section 8 is a discussion of the global impacts that may happen if an El Niño-like response were to occur in a climatological sense. Finally, Section 9 outlines the conclusions reached from this study.

2. PRECOUPLED TESTING

Before the coupled system can be assembled, the GISS AGCM must be tested in an uncoupled mode to see if the AGCM is capable of producing a realistic atmospheric response to observed SST forcing. To accomplish this, the GISS AGCM was run using SSTs obtained from the Atmospheric Modeling Intercomparison Project (AMIP II) as a bottom boundary condition for the period 1979–1988. Monthly wind-stress anomalies from the GISS AGCM were then used to drive the ocean component of the ZC model from 1979–1988 to test how well the AGCM's wind-stress anomaly field generates an El Niño response in the ZC model. The NINO3 SST anomalies from the ZC model driven by the AGCM wind-stress anomalies were than compared to an identical experiment in which the ZC ocean model was driven by observed Florida Sate University (FSU) wind-stress anomalies for the same period (Figure 1). Although the ZC response to the AGCM wind stresses is somewhat weaker than observed, it still produces an appropriate El Niño pattern as indicated by a correlation of 0.72 of Nino3 with respect to AMIP II Nino3, which is significant at the 99% level. A comparison of the AGCM wind-stress anomalies with the FSU wind-stress anomalies in the Nino3 region shows a similar response as the SST Nino3 with a correlation of 0.62 (significant at 99%), although this is also somewhat weaker than observed (Figure 2). The weaker response appears to be a common feature to atmospheric GCMs (McCreary and Anderson, 1991).

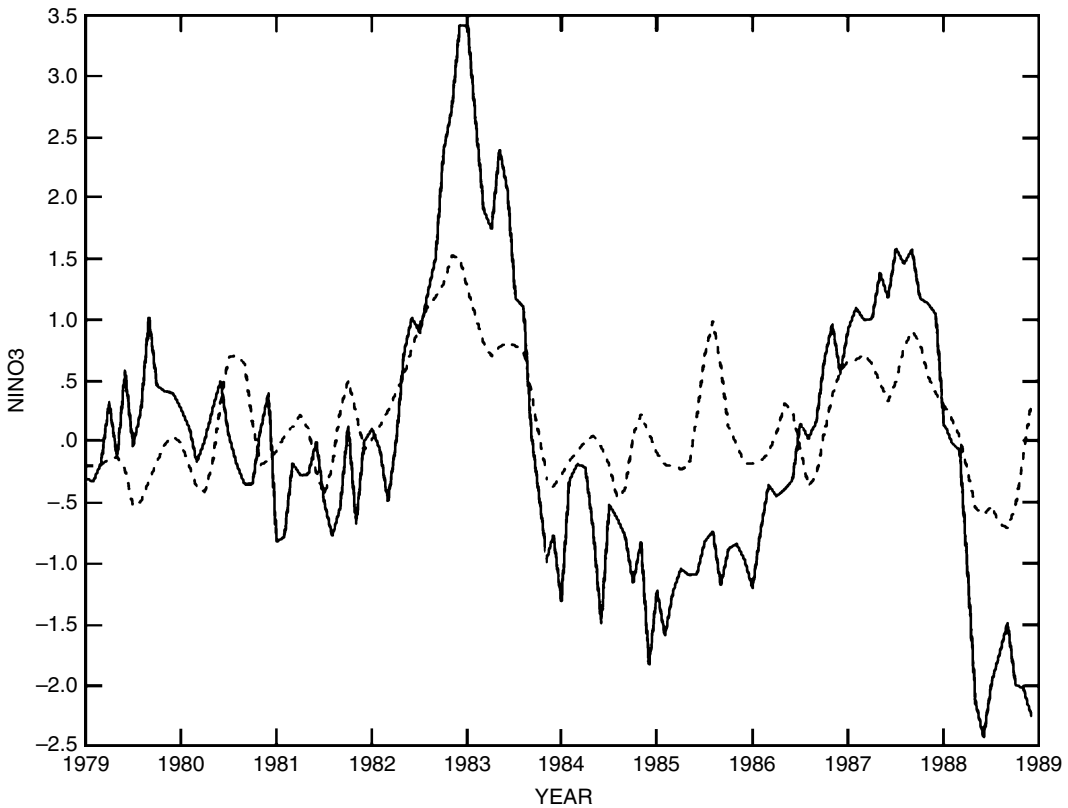

Figure 1. Monthly NINO3 (°C). Solid: from AMIP II, dashed: from ZC model driven by GISS AGCM wind-stress anomalies (AGCM run from 1979–1988 using AMIP SSTs as a bottom boundary condition)

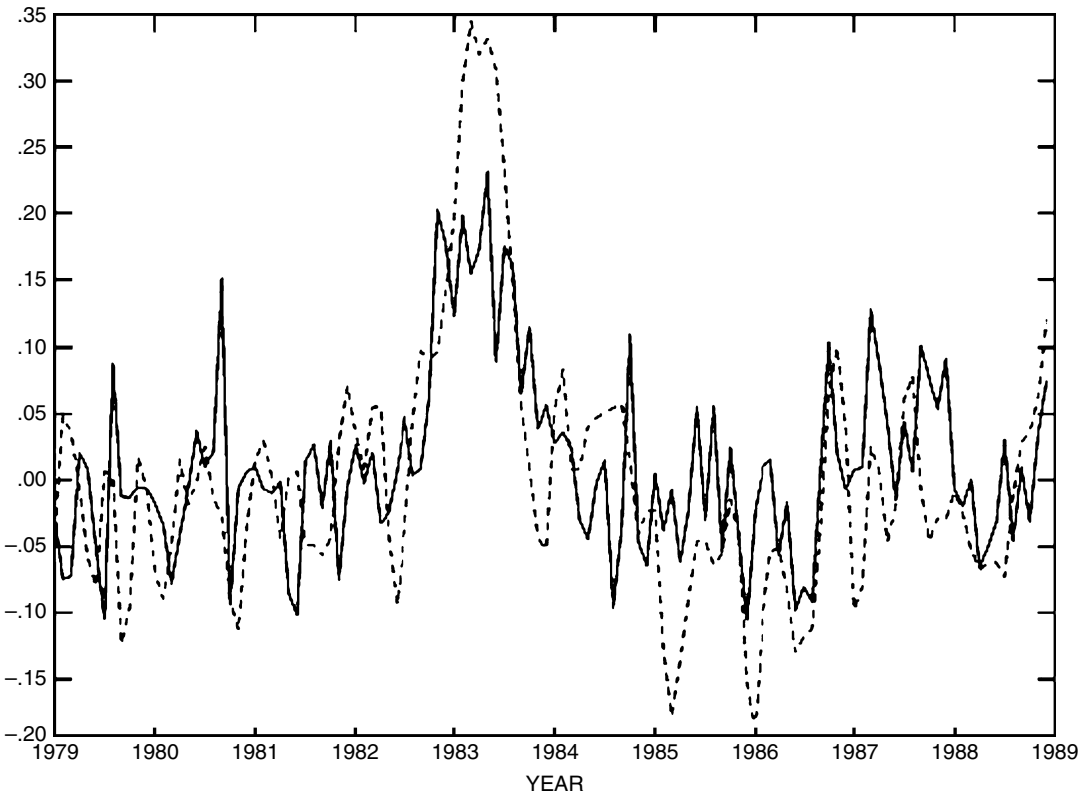

Figure 2. Monthly time series of wind-stress anomalies in the NINO3 region. Solid: from GISS AGCM using AMIP II SST as a bottom boundary, dashed: from FSU wind stress

Despite the AGCM model's weaker wind-stress response to SST forcing than the observed response, the El Niños of 1982–1983 and 1986–1987 are still well-represented. On the basis of this, the following coupling routine was developed to evaluate the model's ENSO capability and the potential to investigate the impacts of global warming on the model's ENSO.

3. COUPLING PROCEDURE

Coupling between the models is illustrated in Figure 3 and proceeds as follows. The AGCMq is run for 10 days (10 days because this represents the ZC model timestep) generating a 10-day averaged surface–wind-stress anomaly field (anomaly generated relative to a previous version of an identical AGCMq run to equilibrium). This wind-stress anomaly field is then interpolated onto the ZC model grid and used as an initial condition in running the ZC model for 10 days. The ZC model in turn produces a surface-ocean dynamical heating component (i.e. surface-ocean heating term due to upwelling), which is interpolated onto the AGCMq model grid and added to the surface heat balance of that portion of the AGCMq domain in which the ZC model operates (i.e. the tropical Pacific). Initially, the AGCMq's SST field can change because of changes only in the vertical flux terms. By adding the surface-ocean dynamical heating term to the q-flux ocean, the AGCMq's SST is allowed to respond not only to vertical heat flux but also to upwelling generated by the AGCMq's own wind-stress anomaly field. This is the equivalent of adding to the AGCMq the physics required to account for the upwelling because of changes in wind-stress anomalies necessary to generate ENSO. The final coupled system consists of the GISS AGCMq, except in the tropical Pacific, where the surface heat balance is altered

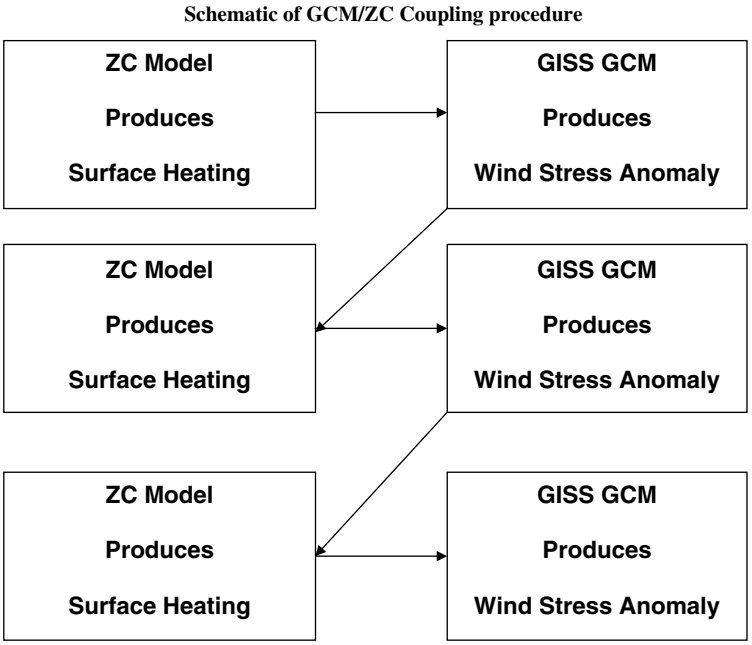

Figure 3. Schematic of GCM/ZC coupled model's computational process

by the inclusion of dynamical heat generated from changes in upwelling in the ZC model. For further details on the coupling physics, please refer to Appendix I.

4. ENSO PHENOMENA

To illustrate the ENSO phenomena produced by the GCM/ZC model, a 50-year simulation of the coupled model was run using the procedure outlined in Section 3 and compared to an identical run of the AGCMq run without the coupling. Figure 4 shows the magnitude of the GCM/ZC model's NINO3 compared with the AGCMq NINO3. The AGCMq produces very little amplitude in the NINO3 region, whereas the coupled model has greater amplitude, to the order of $\pm 1\,^{\circ}$C. This is not surprising because the AGCMq lacks the physics to generate ENSO; namely, that its SST field is only capable of changing because of radiative forcing and lacks the dynamical component (i.e. the SST response due to upwelling) that the GCM/ZC model possesses. While the GCM/ZC model's NINO3 is much improved over the AGCMq, its response is still weaker than the observed response, which typically has NINO3 values ranging from -2 to $+3\,^{\circ}$C. To illustrate the structure of the SST anomalies in the GCM/ZC and AGCMq models, hovmoeller diagrams of the SST anomalies were constructed for a given 10 year period (years 20–30) and are shown in Figure 5. The GCM/ZC model (Figure 5(a)) shows periodic westward propagating SST anomalies appearing approximately every 2 years, indicating the GCM/ZC model's internal ENSO capability while the AGCMq model shows a noisy SST anomaly structure with little propagation (Figure 5(b)). The GCM/ZC's preferred 2-year ENSO periodicity is illustrated in Figure 6(a), which shows a power spectra peak near 2 years. Figure 6(b) shows the frequency of observed ENSO events calculated from the climate prediction center (CPC) observed NINO3 data (http://www.cpc.ncep.noaa.gov/data/indices/sstoi.indices) and shows a preferred peak at 4 years. Neelin *et al*. (1998) note that the spectra of ENSO events has power at all spectral frequencies with preferred peaks approximately at 3–5 and 2 years. The GCM/ZC's shorter frequency of ENSO events relative to the observed events may be attributed to the AGCM's weaker wind-stress anomaly response to SST anomalies implying that the GCM/ZC model has a weaker coupling strength than the observed ocean/atmosphere response. Large wind-stress anomalies indicate a strong coupling strength resulting in a high amplitude/low frequency ENSO

response (Neelin *et al*., 1992; Meehl *et al*., 2001). This is also suggested by Zebiak and Cane (1987) who found that the ZC model responded to increased wind stress by producing El Niños of increased amplitude and periodicity, and by Guilyardi (2005) who found that an increase in coupling strength was accompanied by an decrease in El Niño frequency.

A feature of the GCM/ZC model's ENSO response is a tendency toward westward propagation. To illustrate the behavior of a particular GCM/ZC ENSO event, plots of seasonal SST anomalies and wind-stress anomalies were constructed for a particular ENSO event (specifically, from August–October (ASO) of year 27 of the simulation through May–July (MJJ) of year 29 of the simulation (Figure 7(a)–(h)). The event described can clearly be seen in the hovmoeller diagram of Figure 5(a) (year 27–29, circled). Prior to the beginning of the event in August–October, year 27 (Figure 7(a)), mainly cold SST anomalies span the equatorial Pacific with stronger than normal easterly wind-stress anomalies. By November–January, year 27/28 (Figure 7(b)), positive SST anomalies appear at 105 °W with positive wind-stress anomalies (weaker than normal) west of the warm SST anomaly from 130 to 110 °W. During February–April, year 28 (Figure 7(c)), the positive SST anomalies expand in areal coverage and expand westward to cover an area from 150–90 °W with an area of positive wind-stress anomalies now covering 170–125 °W. During May–July, year 28 (Figure 7(d)), the area of positive SST anomalies continues to expand westward and now covers an area from 180–90 °W although it is now weaker in magnitude. Westerly wind anomalies now extend from 150–110 °W. The event continues to weaken from August–October, year 28 (Figure 7(e)), with positive SST anomalies nearly gone from the equatorial Pacific and wind-stress anomalies reduced in magnitude. During November–January, year 28–29 (Figure 7(f)), the SST anomalies are near (or slightly below) normal in the equatorial Pacific with a suggestion of easterly wind-stress anomalies from 180–150 °W. Finally, February–April, and May–July, year

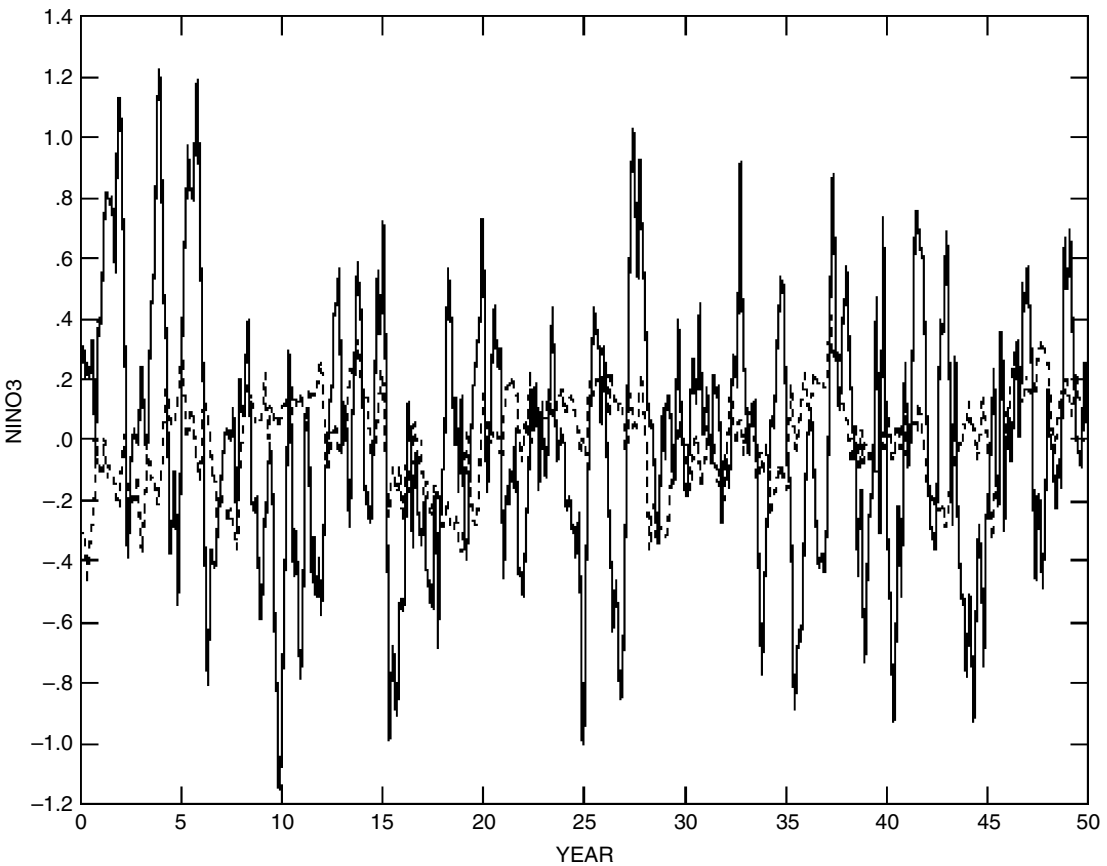

Figure 4. Monthly NINO3 (°C). Solid: from coupled GISS GCM/ZC model, dashed: from GISS AGCMq model

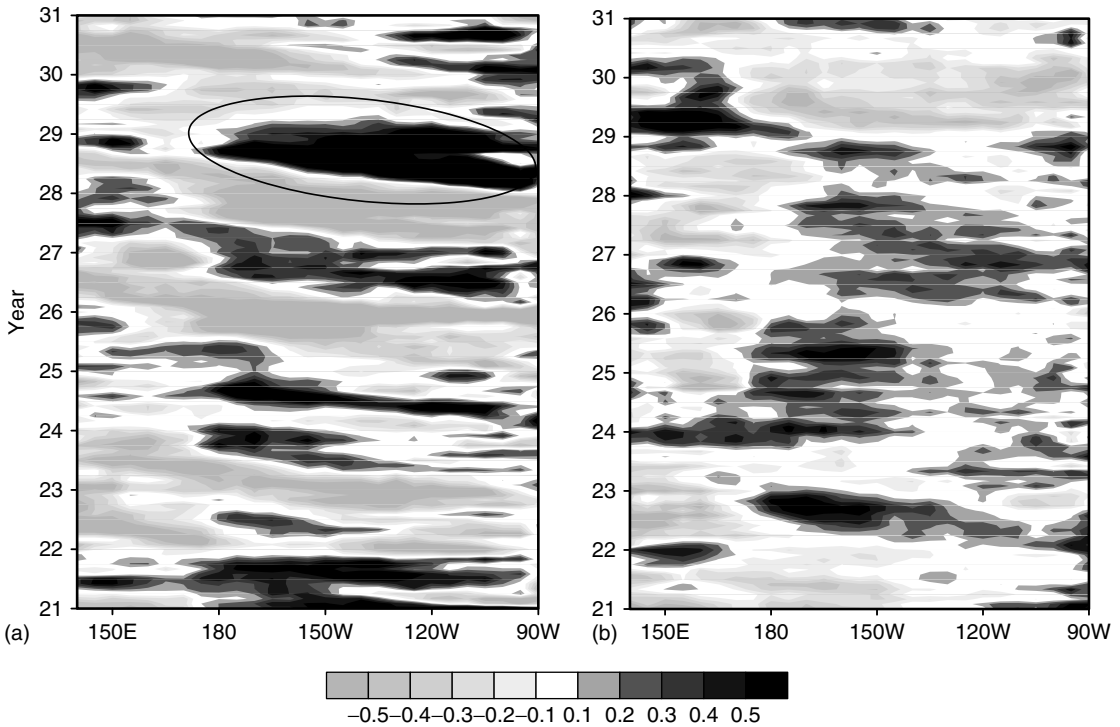

Figure 5. Hovmoeller diagram of monthly sea-surface temperature anomalies (°C) taken at 2 °S for the year 20-year 30 period from (a) coupled model and (b) q-flux model anomalies derived from monthly mean climatologies over 50 years. Circled area in Figure 5(a) represents the El Niño event analyzed in Figure 7

29 (Figure 7(g), (h)), show somewhat cooler than normal SST in the equatorial Pacific and near normal/slightly stronger than normal easterly anomalies associated with neutral/weak La Niña conditions.

The mechanism responsible for ENSO-like variability in the GCM/ZC model is similar to the description given in Rasmusson and Carpenter (1982) and is likely related to the mechanisms described by Battisti (1988). Battisti (1988) related the growth of equatorial Pacific SST anomalies to several terms in the SST equation; namely, zonal advection of SST from the west and upwelling of anomalously warm subsurface water due to thermocline suppression in the east. This is also indicated in some of the modeling studies described in Neelin *et al*. (1998). By including these processes inherent in the ZC component of the model, the GCM/ZC model is able to produce a specific mode of ENSO response.

In the Northern Hemisphere, the appearance of a warm event during the fall season, followed by a winter peak, and then a decline during summer shows that the GCM/ZC model has locked in fairly well with the annual cycle, although Zebiak and Cane (1987) demonstrate that events tend to amplify sharply in the Northern Hemisphere summer. The late amplification of the GCM/ZC event (Fall) may be related to the weaker coupling strength of the GCM/ZC model (i.e. weaker wind-stress anomalies forcing the ZC model) although more investigation is needed to identify the cause.

5. GLOBAL TELECONNECTIONS

Since the GCM/ZC model produces a coherent ENSO response, it is prudent to investigate if it is capable of producing an appropriate global atmospheric response; this is especially important when evaluating the GCM/ZC model's climate during the global-warming simulations in Section 8. It is well known that ENSO impacts global weather (see Trenberth *et al*., 1998 for a good description). Some of the ENSO-related weather

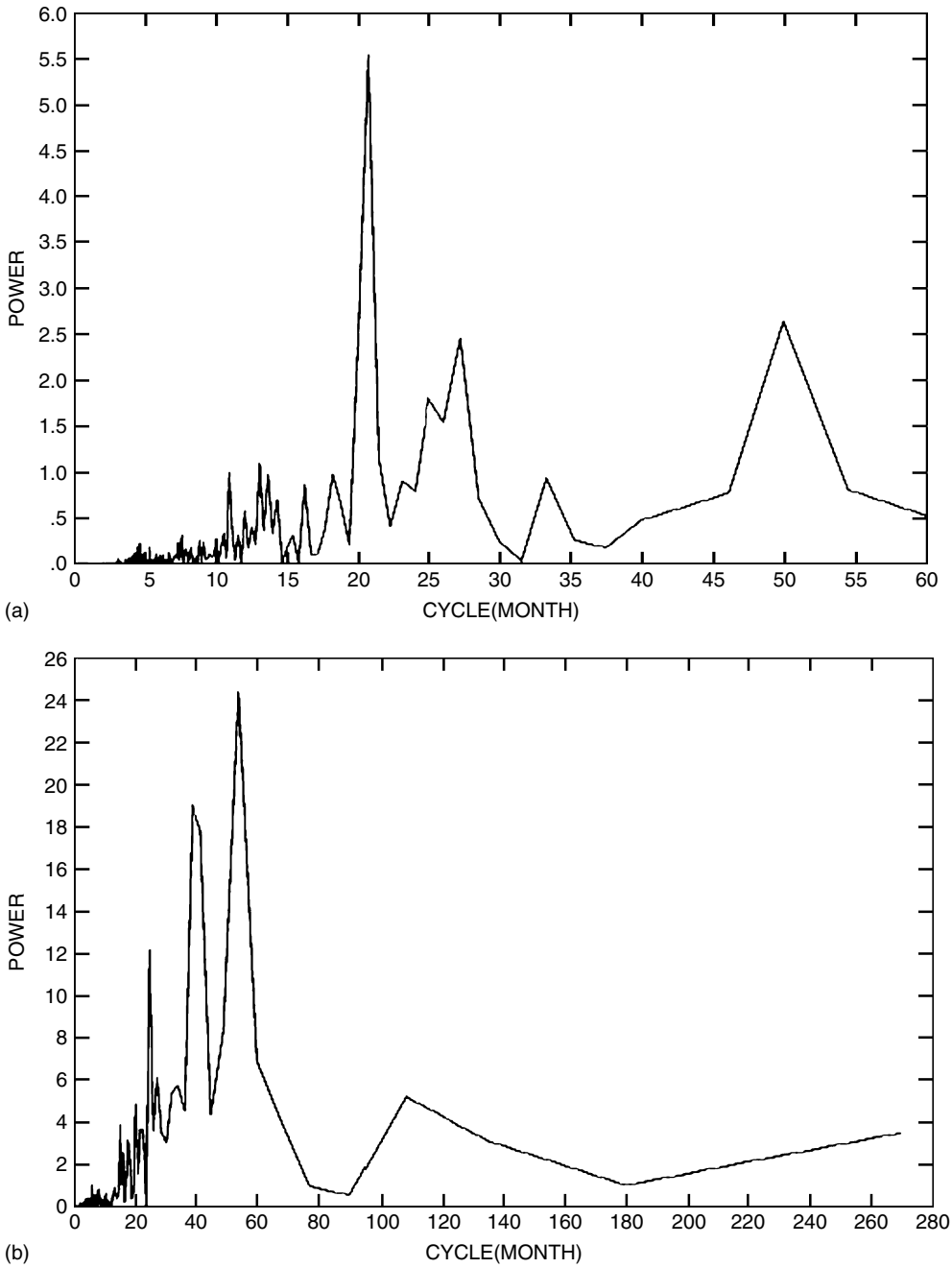

Figure 6. Power spectra derived from monthly NINO3 time series of sea-surface temperature anomalies (a) coupled GISS GCM/ZC model; (b) observed SST

phenomena include Indonesian and South African drought, increased rainfall in Peru and the southern United States, increased East Pacific hurricanes, decreased Atlantic hurricanes, generally mild winters across much of the United States, and increased storminess across the United States west coast. Much of the anomalous weather produced in the United States in winter is because of the predominance of the Pacific North American (PNA) pattern during ENSO. Kumar and Hoerling (1997) composited observed winter 500 hPa height anomalies for the seven largest El Niños in the period 1950–1994 and compared it with an identical composite

from a GCM (Figure 10). They found that the model response was weaker than observed, attributable to either model error or as an artifact because of averaging over a large number of runs (13-member ensemble mean). A similar analysis was done with the GCM/ZC model for winter using NINO3 > 0.5 as a limit for El Niño and NINO3 < -0.5 for La Niña (Figure 9). Since the GCM/ZC's ENSO response is weaker than the observed, using a compositing value of 0.5 for NINO3 is appropriate and represents approximately one standard deviation of NINO3 variability. The spatial structure of the GCM/ZC 500 hPa pattern obtained via compositing analysis (Figure 9) agrees well with observations with lower heights across the North Pacific and southern United States and higher heights over Canada; though weaker than the observed (Figure 8(a)). For La Niña, the opposite pattern of height anomalies occur. Not surprisingly, the GCM/ZC response to SST anomalies is weaker than the observed, mostly because of the GCM/ZC's smaller El Niño amplitude relative

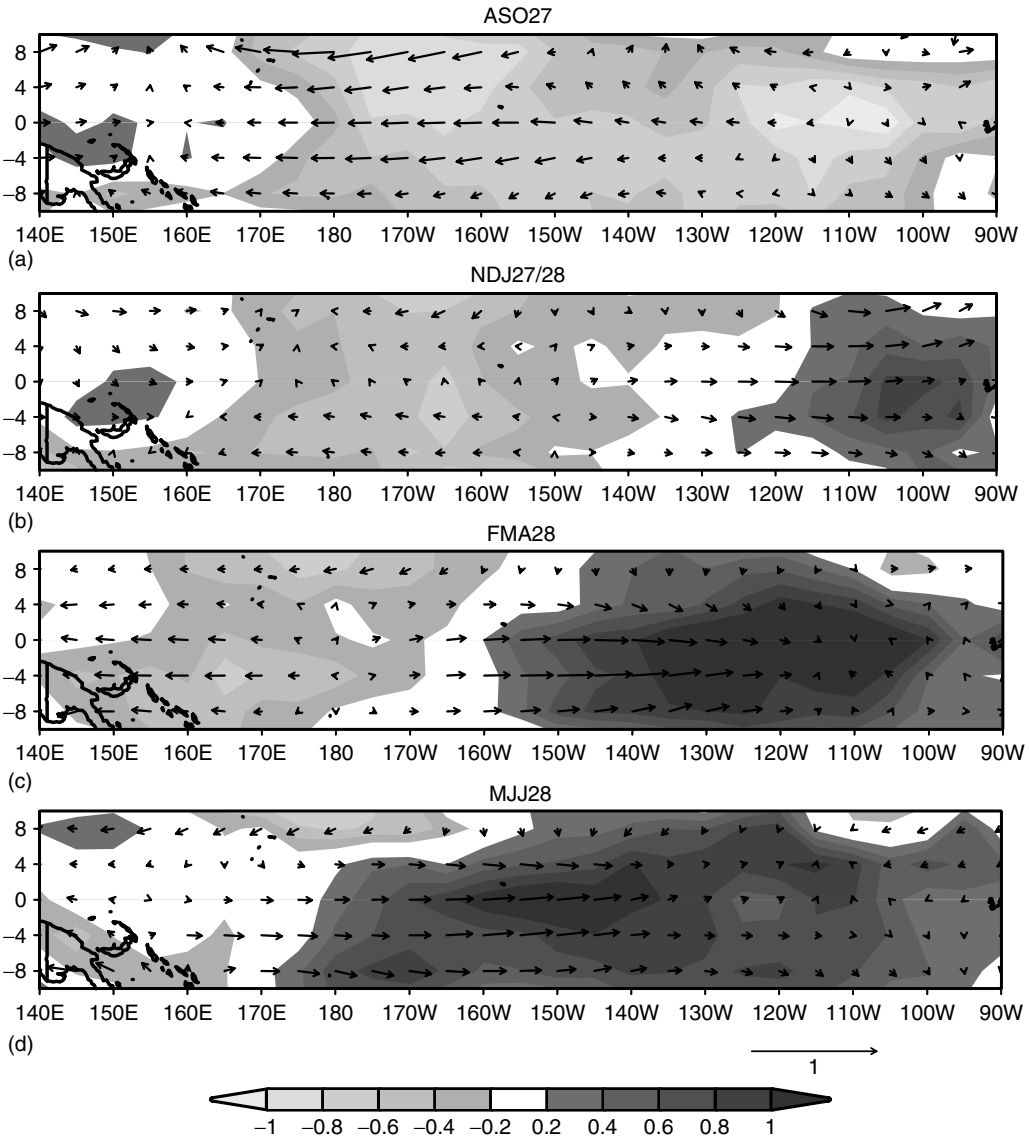

Figure 7. Sea-surface temperature anomaly (shaded, °C) and wind-stress anomalies (vector, dyne/cm^2) for a particular El Niño event (circled in Figure 5(a)) spanning years 27–29 from the 50-year simulation of the GCM/ZC model, (a) ASO27; (b) NDJ27/28; (c) FMA28; (d) MJJ28; (e) ASO28; (f) NDJ28/29; (g) FMA29; (h) MJJ29

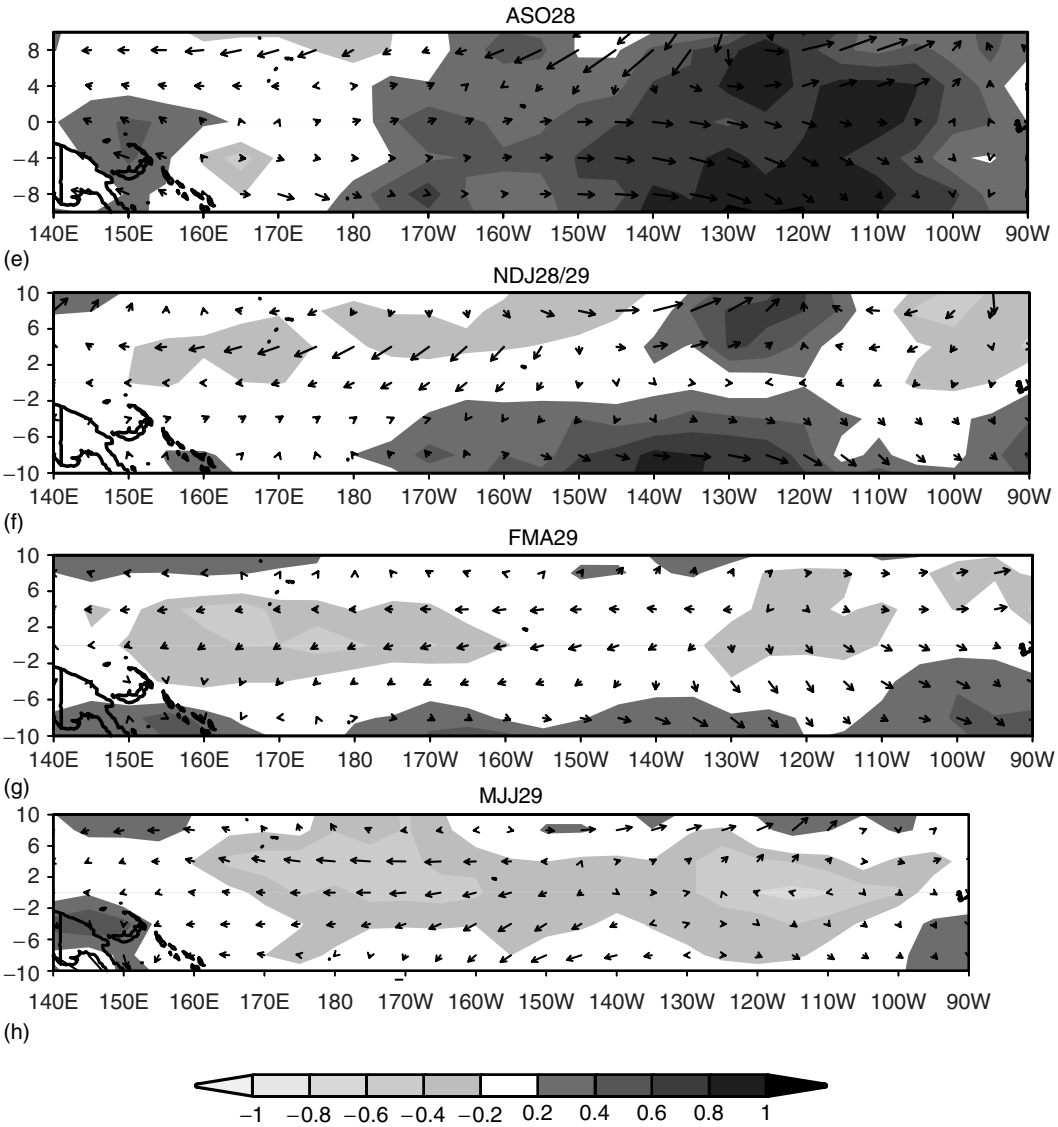

Figure 7. (*Continued*)

to the observed. However, since Kumar and Hoerling (1997) also obtained a weaker response using observed SST forcing, model physics may also play a role, specifically referring to the AGCM's response to surface heating.

In a similar fashion as the 500 hPa height anomalies, winter composites were also constructed for precipitation and 200 hPa. zonal wind (Figures 10 and 11). Winter ENSO conditions are normally associated with increased (decreased) precipitation in the eastern Pacific, less (more) precipitation in the western Pacific and northeastern Brazil, and increased (decreased) precipitation across the southern United States during El Niño (La Niña). As seen in Figure 10(a) and (b), the GCM/ZC model simulates these features quite well. In addition, El Niño (La Niña) causes a strong (weak) subtropical jet stream, which influences stormtracks across the southern United States. Figure 11(a) and (b) show a similar response to the GCM/ZC's 200 hPa wind anomalies for El Niño and La Niña conditions respectively.

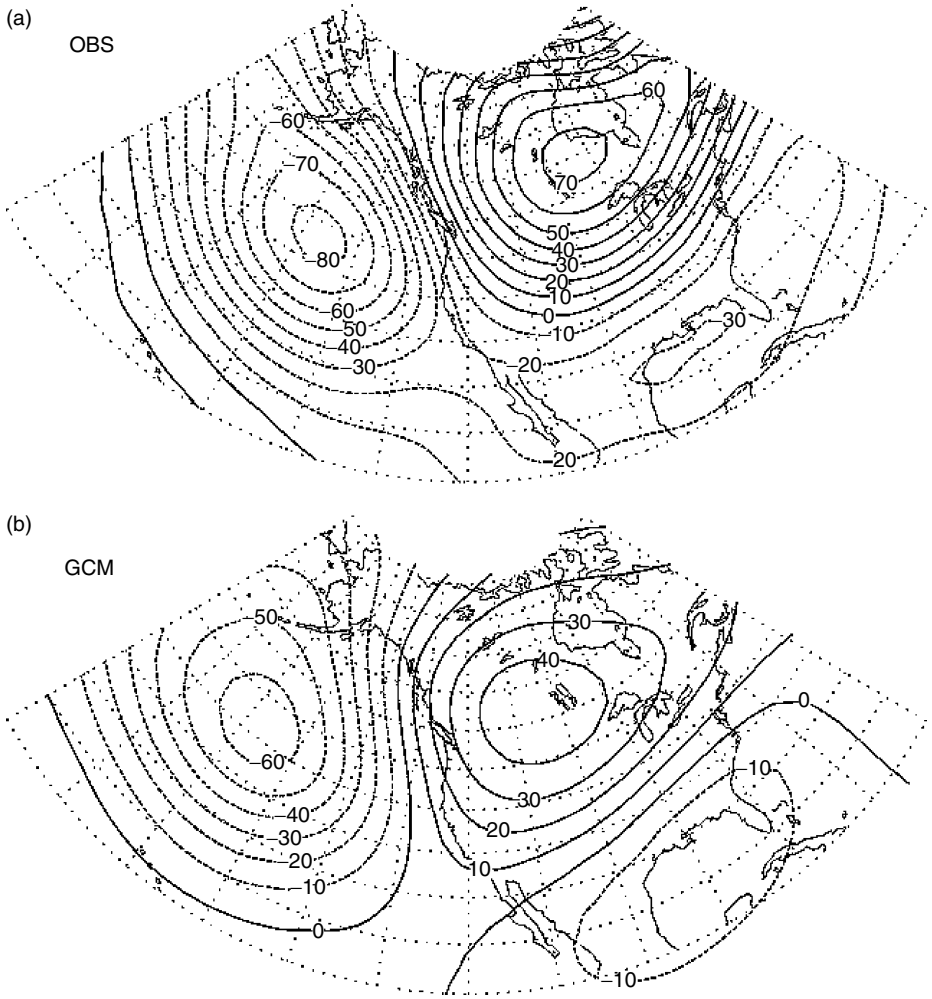

Figure 8. 500 hPa height anomaly composites for (a) El Niño and (b) La Niña from Kumar and Hoerling (1997)

6. GLOBAL-WARMING SIMULATIONS

The focus of the global warming portion of this work is to discuss how certain physical processes (especially upwelling) impact ENSO variability/intensity. To accomplish this, the GCM/ZC and AGCMq models were evaluated for $2 \times CO_2$ and $4 \times CO_2$ equilibrium climates, which was achieved by increasing atmospheric concentrations of CO_2 one percent per year for 70 (140) years for $2 \times CO_2$ ($4 \times CO_2$) and then run for an additional 70 years keeping atmospheric CO_2 concentrations constant. The last 50 years of each run was chosen to represent the equilibrium climate states described here. Comparisons are made to two base $1 \times CO_2$ runs, the GCM/ZC and AGCMq 50-year simulations.

A key physical aspect of the ENSO response to global warming is the temperature of the upwelled water. Since the STC represents a mechanism by which heat is transported to the equatorial mixed-layer, a crude representation of the STC is included in some of the simulations by generating 5-year running means of the SST difference between the global-warming simulation and the original control run averaged over the subtropical North and South Pacific (160–130 °W, 20–40 °N; 20–44 °S, 160–130 °W for North and South Pacific respectively) averaging the northern and southern components together and adding the difference to the temperature at the base of the mixed layer in the ZC model; this effectively alters the vertical temperature gradient which can then change SST via upwelling. The regions of the subtropical Pacific as the source areas

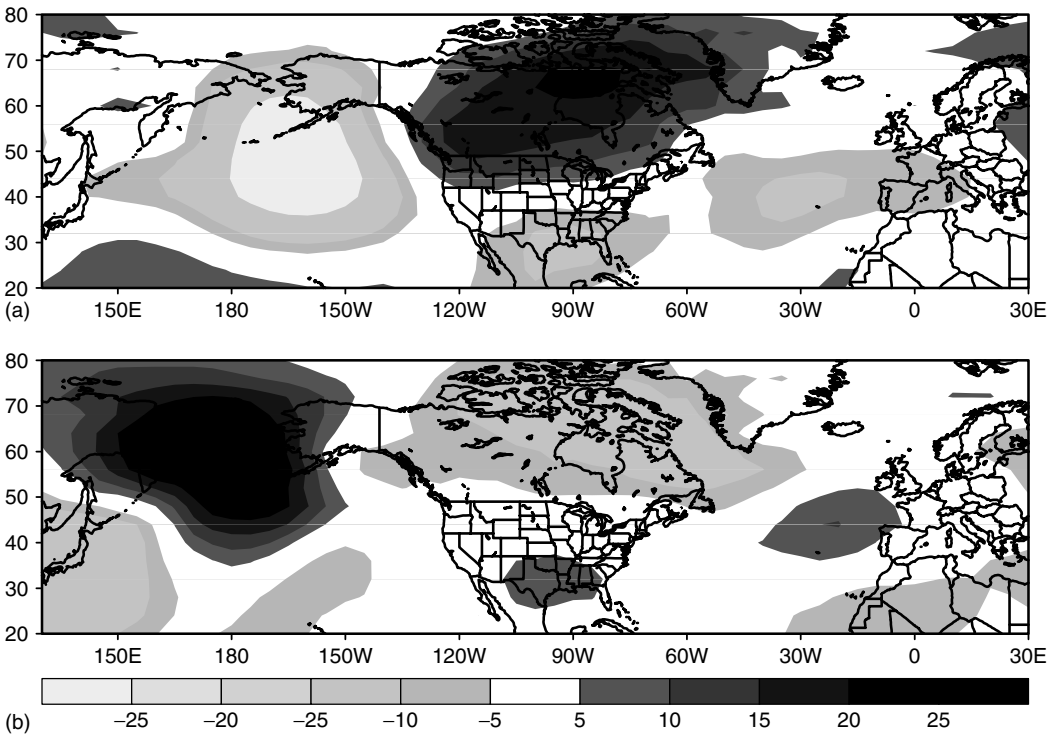

Figure 9. GCM/ZC composite 500 hPa height anomalies (m) for winter (DJF). (a) average of all winters for which NINO3 > 0.5 and (b) average of all winters for which NINO3 < -0.5

were chosen on the basis of the idea that the water reaching the equator originates in the northeastern and southeastern subtropical Pacific at approximately 155 °W, (McCreary and Lu, 1994 and Liu, 1994). Further evidence of southern source water originating in the subtropical southeastern Pacific is given by Wong and Johnson (2003) who indicated source regions on the basis of data from the World Ocean Circulation Experiment at 32 °S west of 140 °W and 32 °S between 115 and 85 °W. Given that there is some uncertainty in the exact location of source water for the STC, the areas used in this study serve as a fair approximation of the STC parameterization.

To demonstrate the warming that occurs in the subtropics due to the increase in CO_2 in the absence of dynamical forcing, an annual average of SST, averaged over the northern and southern regions described above, were computed for the transient GCM/ZC $4 \times CO_2$ run with no STC forcing (Figure 12). It is clear that SST in the subtropical regions steadily increase while the CO_2 increases (140 years) followed by equilibration in the last 50–60 years of the run at approximately 25 °C. It is this increase in temperature that supplies the heating to the equatorial mixed-layer in the STC runs. Since the return period of the water in the STC and where the water appears in the equatorial zone are not clear (e.g. Kleeman *et al.*, 1999 shows the speed may vary) the heating term is added uniformly to the equatorial mixed-layer east of 130° with a time lag of 15 years (approximate time for the heat from the surface in the subtropics to reach the equatorial mixed-layer in the STC). In this fashion, year 18 of the simulation receives heat from the subtropics averaged from years 1 to 5 (i.e. centered on year 3), year 19 from years 2 to 6 (centered on year 4), and so on. To evaluate the importance of the STC in the final equilibrium solutions of the $2 \times CO_2$ and $4 \times CO_2$ runs, comparisons are made to identical runs without inclusion of the STC.

As explained in the introduction, although it is beyond the scope of this paper to outline a specific mechanism by which the STC adds heat to the equatorial mixed-layer, the runs including the STC are to be considered as a sensitivity study which assumes that all heat from warming of the SST in the subtropics eventually arrives in the equatorial mixed-layer so as to delineate the potential climate impacts because of altered ENSO

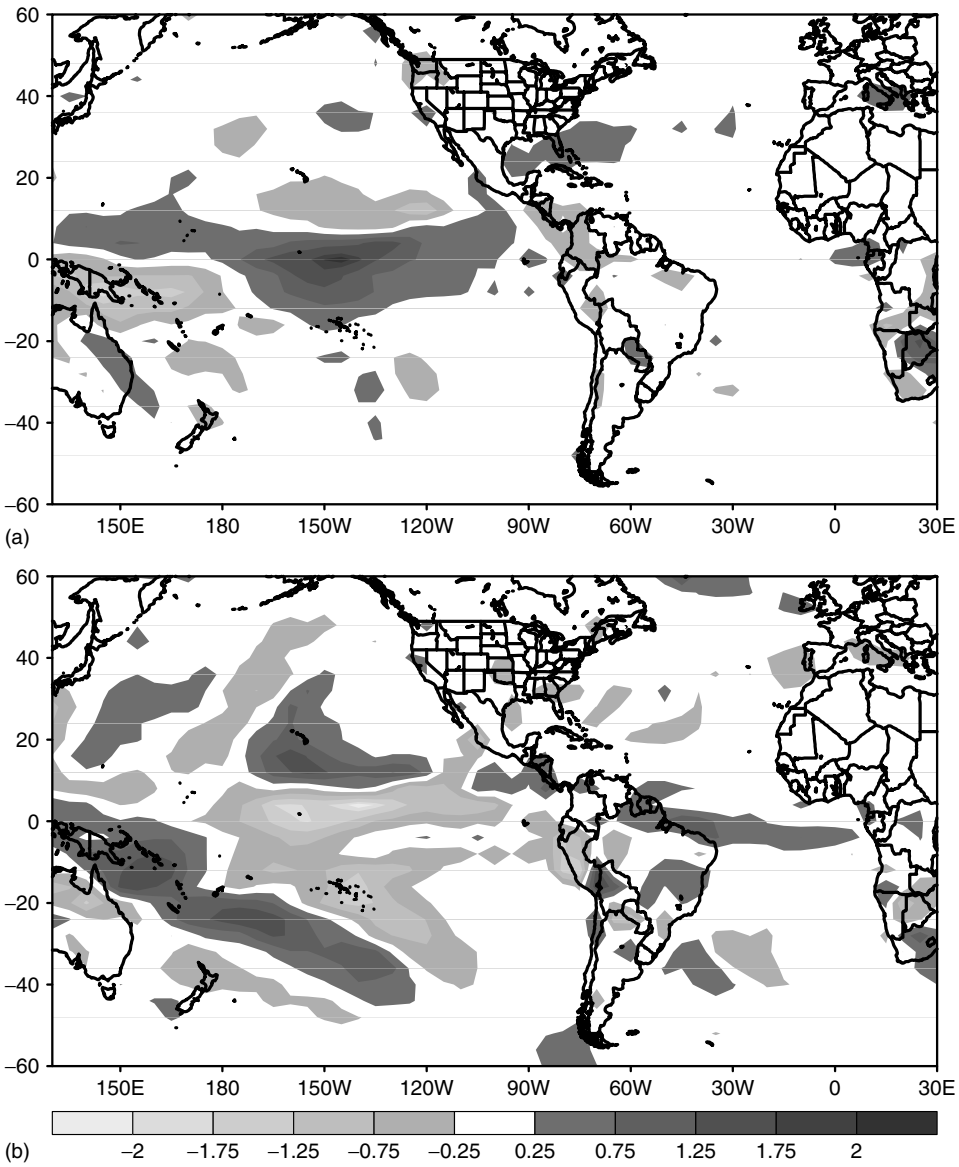

Figure 10. Like Figure 9, except for precipitation anomalies (mm/day)

variability due to global warming. Note that heat is neither added nor subtracted from the subtropical ocean (thus conserving energy) while heat added to the mixed layer of the ZC model is assumed to be upwelled and advected via the ZC model's three-dimensional temperature advection in the form of specified mean currents and ZC-generated anomalous currents. Current and future improvements in models and observations will provide a better understanding of the physical mechanisms of the structure of the STC, which will help quantify how much heat is transported to the equatorial mixed-layer via the STC.

7. GLOBAL-WARMING IMPACT ON ENSO FREQUENCY/AMPLITUDE

To illustrate how global warming impacts ENSO amplitude, the annual average of the NINO3 SST (not the anomaly) for the $4 \times CO_2$ run is given with and without inclusion of the STC, as well as for a $4 \times CO_2$ run

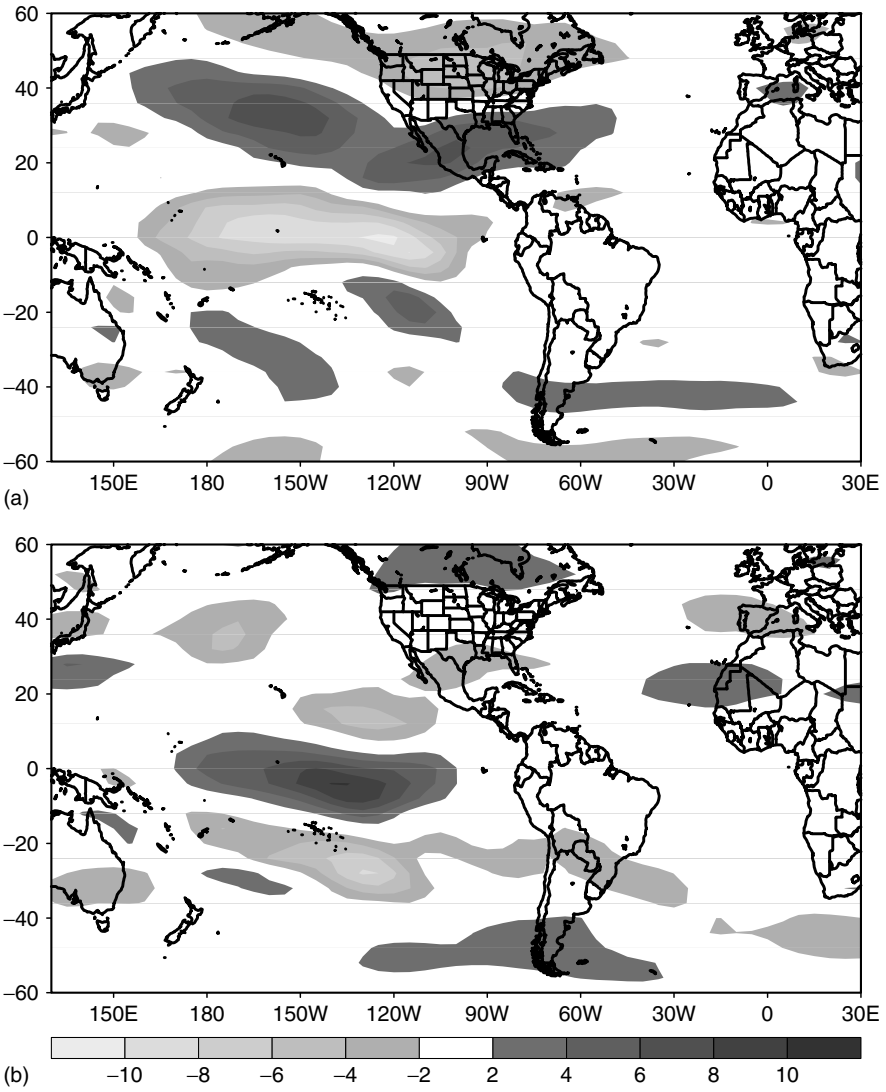

Figure 11. Like Figure 9, except for 200 hPa. Wind anomalies (m)

of the AGCMq. (Figure 13). The AGCMq and the GCM/ZC with no STC inclusion exhibit similar behavior although the GCM/ZC without the STC has greater interannual variability. However, both runs equilibrate near 31 °C. For the GCM/ZC run with the STC, the added heat from the STC begins to have effect approximately in the year 2030 indicated by the greater increase in SST relative to the other runs. An interesting feature of the GCM/ZC run with the STC is an increase in interannual variability from approximately 2030–2070. To investigate this apparent increase in interannual variability, a 3rd order regression function was used to detrend the 3 curves in Figure 13. The standard deviation for the detrended data curve was then computed; NINO3 SST anomalies were then computed from the detrended data. Figure 14 shows the detrended NINO3 anomalies for the first 140 years of each run, with the dashed lines indicating two standard deviation limits. For the AGCMq and GCM/ZC without the STC (Figure 14(a) and (b)), there is no discernable pattern in the anomalies; although often hitting the two standard deviation lines, it appears to happen randomly throughout the transient phase of each run. For the GCM/ZC with the STC, a specific pattern emerges with the anomalies generally staying below the two standard deviation lines until the year 2030 (approximately within ±0.5 °C); however, from 2030 to 2090, the anomalies often hit the two standard deviation lines (doubling to ±1 °C) indicating a

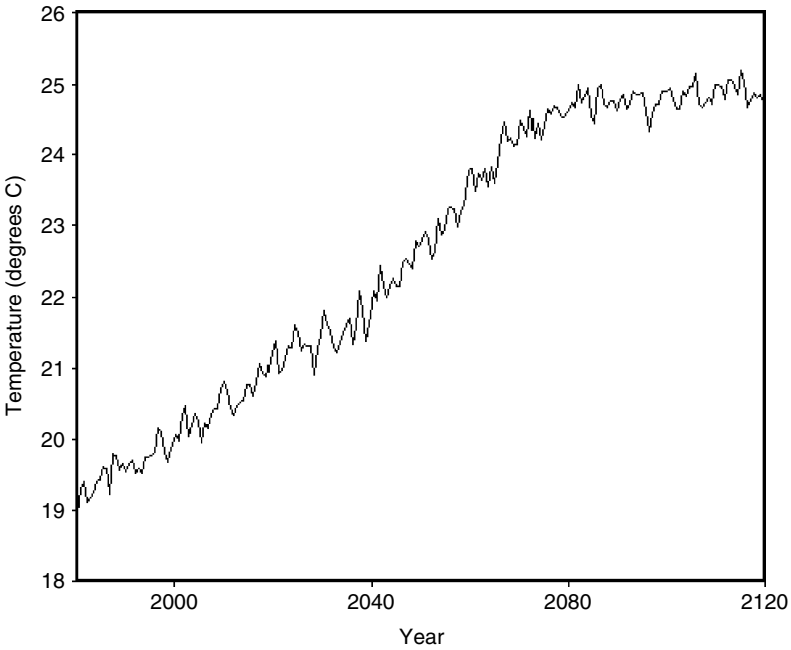

Figure 12. Mean annual SST averaged over (20–44 °N,160–130 °W), (20–44 °S, 160–130 °W) from $4 \times CO_2$ coupled GCM/ZC run with no STC. Area represents that used for STC inclusion

significant increase in amplitude. Finally, after year 2100, the amplitude decreases with anomalies reduced to approximately ±0.5 °C. A potential physical explanation for this behavior is described by Timmerman *et al*. (1999) who suggested that a stronger Hadley circulation in response to global warming may initially result in a greater inflow of colder water resulting in an increase in amplitude; however, as climate continues to become warm, this inflow becomes increasingly warm (in this case from the STC) and results in a decrease in amplitude. A decrease in amplitude was also found by Collins and the CMIP Modeling Groups (2005), Merryfield (2005), and Meehl *et al*. (2005). However, Guilyardi (2005) found an increase in amplitude in response to a warmer climate when examining multimodel ensembles.

Another feature of Figure 14 is the greater interannual variability of the GCM/ZC runs (with and without the STC) relative to the AGCMq run. Table I shows the monthly NINO3 standard deviation for the equilibrium climates for all of the $1 \times CO_2$ and $4 \times CO_2$ runs described in this study. Note that the equilibrium climates are defined as years 1–50 for the $1 \times CO_2$ runs, years 90–140 for the $2 \times CO_2$ runs, and years 160–210 for the $4 \times CO_2$ runs. From Table I, a specific pattern emerges; the greatest variability is illustrated by the $1 \times CO_2$ GCM/ZC run; the $4 \times CO_2$ GCM/ZC without the STC has slightly more variability than the $4 \times CO_2$ run with the STC; finally the $1 \times CO_2$ and $4 \times CO_2$ AGCMq runs have the lowest variability. While it is not surprising that the AGCMq runs have the lowest variability, it is interesting that the $4 \times CO_2$ coupled runs have reduced interannual variability relative to the $1 \times CO_2$ GCM/ZC model. A possibility is that warming of the equatorial Pacific reduces the intensity of the cold tongue, which acts to reduce the wind-stress anomalies leading to a further decrease in coupling strength relative to the $1 \times CO_2$ GCM/ZC run. To assess this possibility, the mean SST for winter (DJF) for the western Pacific (defined as 5 °N–5 °S, 150 °E–180 °E) was subtracted from the eastern equatorial Pacific (defined as 5 °N–5 °S, 150 °W–90 °W) for all of the equilibrium climates of the $1 \times CO_2$, $2 \times CO_2$, and $4 \times CO_2$ runs (Table II). All of the runs maintain a cold tongue except the runs with the STC. In fact, the $4 \times CO_2$ run with the STC reverses the cold tongue completely. This is because of the alteration of the vertical temperature gradient from an increase in temperatures at the base of the ZC mixed layer via the STC parameterization, which effectively destroys the longitudinal SST gradient. Another interesting feature can be seen by comparing the $4 \times CO_2$ SST gradients for the runs without the STC (i.e. AGCMq

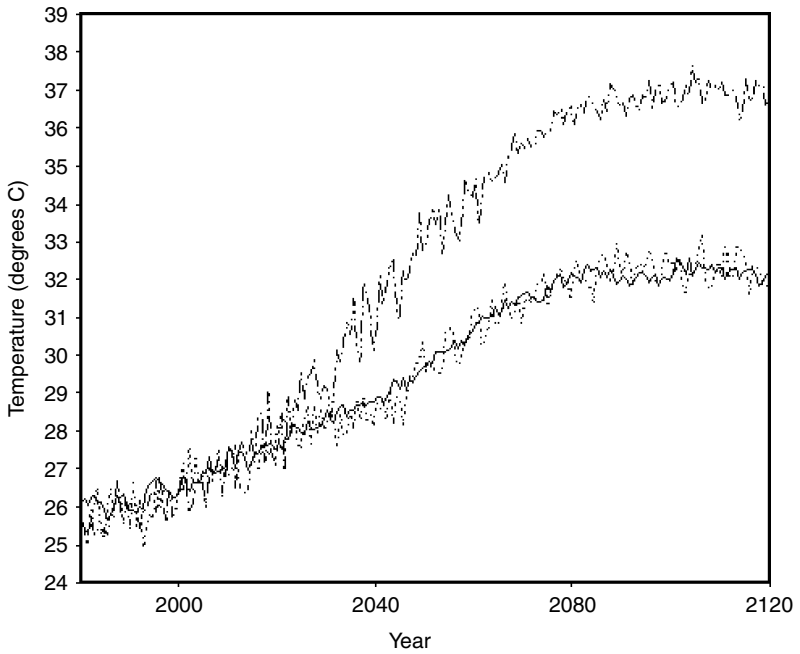

Figure 13. Annual mean time series of NINO3 (°C), solid: AGCMq dashed: GCM/ZC with no STC Dot-dashed: GCM/ZC with STC

and ZC/GCM without the STC) with the $1 \times CO_2$ runs. For the q-flux runs, the longitudinal SST gradient reduces from $-1.75\,^{\circ}C$ to $-1.15\,^{\circ}C$ when quadrupling CO_2 while for the coupled simulations without the STC, it reduces from $-0.96\,^{\circ}C$ to $-0.8\,^{\circ}C$. As noted by Meehl *et al.* (2000), this is a common feature in GCMs perturbed by increased CO_2 and may be because of the effects of cloud forcing. Another possible mechanism is that the evaporative feedback mechanism may be operative as suggested by Knutson and Manabe (1995)

To evaluate the spatial changes in equatorial Pacific SST/wind stress due to global warming in more detail, the mean DJF SST/wind stress was calculated for each of the coupled runs. To separate the effects of radiative forcing from impact due to the STC, two sets of climatologies are shown. Figure 15 shows the $1 \times CO_2$, $2 \times CO_2$ and $4 \times CO_2$ mean SST/wind-stress climatologies for the equilibrium components of the simulations (years 1–50 for $1 \times CO_2$ run, years 90–140 for the $2 \times CO_2$ run, and years 160–210 for the $4 \times CO_2$ run). Figure 15(a) shows that for the $1 \times CO_2$ run, a longitudinal SST gradient depicting the cold tongue exists across the equatorial Pacific, accompanied by mean easterly wind stresses. In contrast, the $2 \times CO_2$ solution shows a significant warming of the central equatorial Pacific accompanied by a weakening of the wind stress (Figure 15(b)). Finally, the $4 \times CO_2$ case (Figure 15(c)) shows an El Niño-like response with a disappearance of the easterly wind stress across the equatorial Pacific. Differencing the final $2 \times CO_2$ and $4 \times CO_2$ states with the $1 \times CO_2$ run (Figure 16(a) and (b)) display the decrease in wind stress in

Table I. Standard deviation of mean monthly terms in NINO3 region

	SST (°C)
$1 \times CO_2$ (coupled)	0.52
$4 \times CO_2$ (coupled, no STC)	0.37
$4 \times CO_2$ (coupled, with STC)	0.30
$1 \times CO_2$ (q-flux)	0.16
$4 \times CO_2$ (q-flux)	0.18

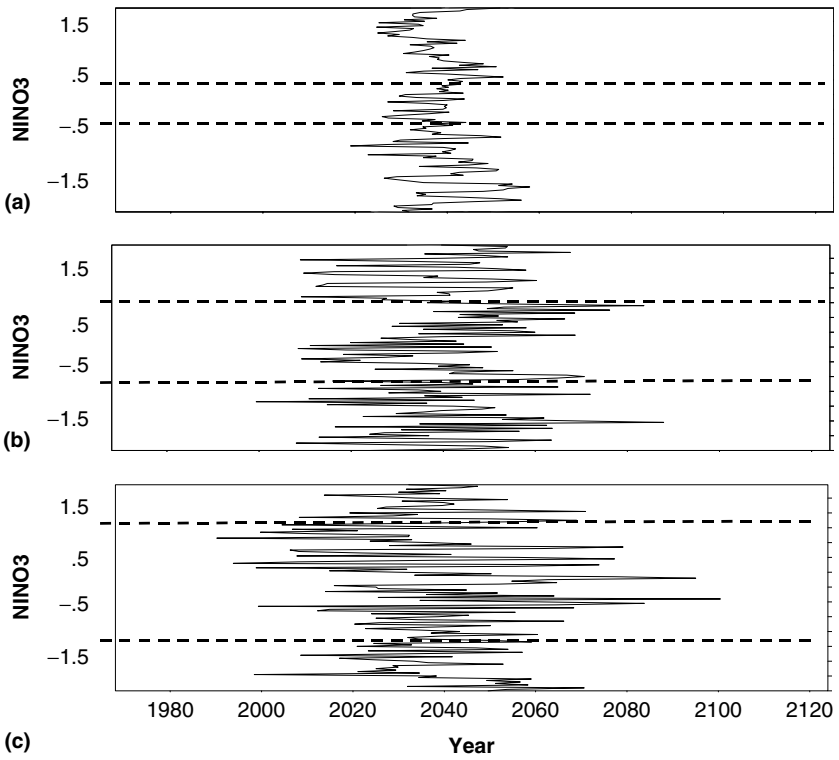

Figure 14. Annual NINO3 anomalies (°C) from $4 \times CO_2$ runs for (a) q-flux; (b) coupled model without STC; (c) coupled model with STC. NINO3 values are for transient portion of run and are derived from mean calculated from 3rd order polynomial regression. Dashed lines represent 2 standard deviation limits about the mean

Table II. Mean annual SST difference E. Pacific (5 °N–5 °S, 150–90 °W)–W. Pacific (5 °N–5 °S, 150 °E–180 °W)

Run	ΔSST (E–W) °C
$1 \times CO_2$ (Coupled)	−0.96
$1 \times CO_2$ (q-flux)	−1.75
$2 \times CO_2$ (Coupled with STC)	−0.85
$4 \times CO_2$ (Coupled with STC)	+0.27
$2 \times CO_2$ (Coupled with no STC)	−0.90
$4 \times CO_2$ (Coupled with no STC)	−0.80
$4 \times CO_2$ (q-flux)	−1.15

the equatorial Pacific along with a warming of the ocean especially concentrated in the equatorial central Pacific ranging from approximately 6 °C for the $2 \times CO_2$ run (Figure 16(a)) to more than 10 °C for the $4 \times CO_2$ run (Figure 16(b)). Although this is an extreme example of the impact of changes in the STC on the equatorial Pacific, it is appropriate to contemplate what even a modest addition of heat to the equatorial Pacific would imply for ENSO and global climate. The second set of climatologies is like the first except that it is done for the runs without the inclusion of the STC (Figure 17(a)–(c)). For the runs without inclusion of the STC, the longitudinal equatorial Pacific SST gradient is generally maintained for the $2 \times CO_2$ and $4 \times CO_2$ cases (Figure 17(b) and (c)) similar to the $1 \times CO_2$ run (Figure 17(a)), although some weakening of the wind stress is noted west of the dateline for the $4 \times CO_2$ run (Figure 17(c)). Differencing the $2 \times CO_2$ and $4 \times CO_2$ runs with the $1 \times CO_2$ run Figure 18(a) and (b)) show a uniform

warming with little change in wind stress for the $2 \times CO_2$ run relative to $1 \times CO_2$ indicating a maintenance of the longitudinal SST gradient (albeit at a higher temperature); for the $4 \times CO_2$ run relative to $1 \times CO_2$, there is slightly more warming in the eastern Pacific relative to the west, although not enough to destroy the gradient.

Interestingly, the warming in the eastern Pacific is centered south of the equator (accompanied by a weakening of wind stress from the equator south into the south-tropical Pacific). This indicates a reduction of the coupling strength and helps to explain the decrease in interannual variability of NINO3 relative to the $1 \times CO_2$ run. It is clear from these analyses that the STC mechanism as parameterized crudely in these simulations plays a significant role in the destruction of the longitudinal SST gradient leading to the GCM/ZC model's El Niño-like response. Although the efficiency of the ability for the STC to transport heat is a source of uncertainty, coupled model simulations, feedback analysis, and paleoclimate reconstructions suggest an El Niño-like response due to radiative forcing from increased atmospheric CO_2 concentrations (Boer *et al.*, 2004).

Finally, it should be noted that the El Niño-like response obtained in the STC runs also have a positive impact on global warming. Figure 19 shows the global surface-air temperature (SAT) plotted for the $4 \times CO_2$ runs with and without inclusion of the STC (solid and dashed lines respectively). It clearly illustrates that the runs with the STC warm more rapidly than the runs without the STC, with the final equilibrium temperature

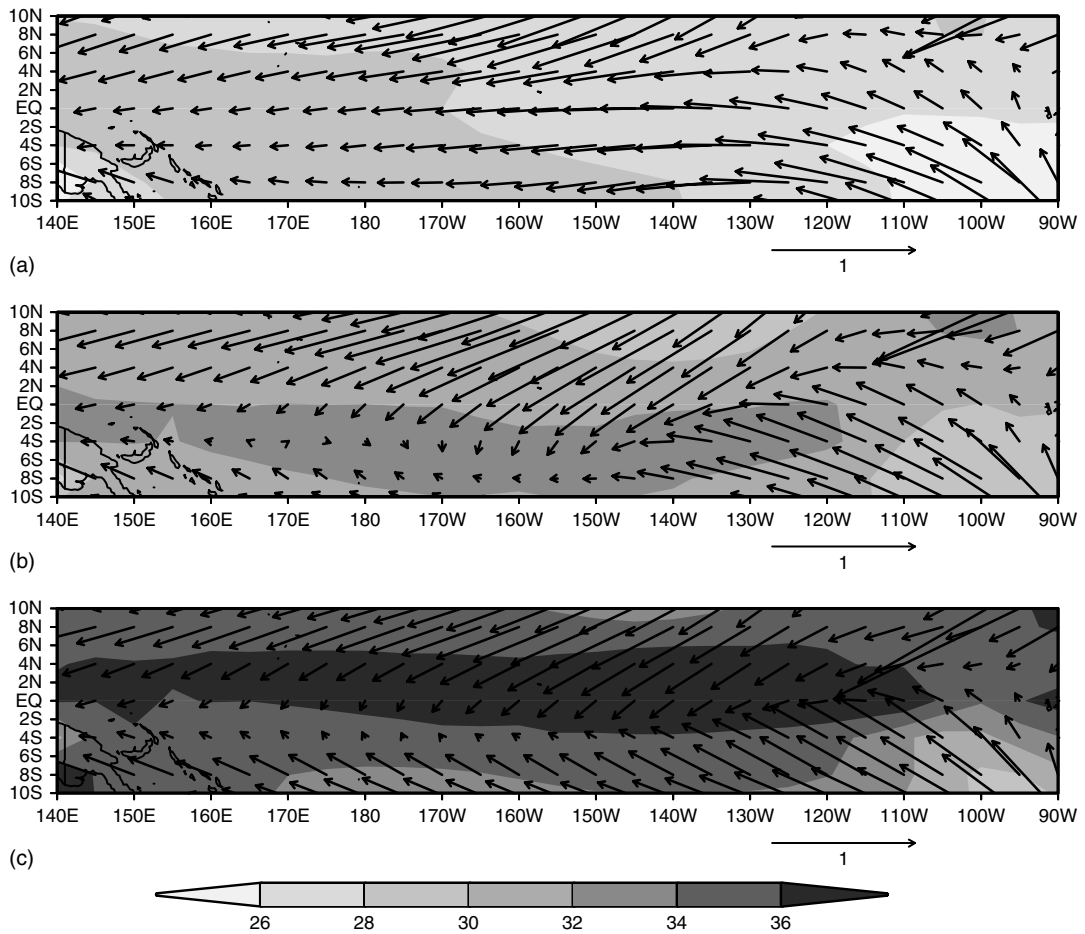

Figure 15. DJF sea-surface temperature (shaded, °C) and wind stress (vector, dyne/cm^2) for (a) 50 year Mean annual average of $1 \times CO_2$ coupled model; (b) Year 90–140 average of $2 \times CO_2$ coupled model simulation with STC; (c): Year 160–210 average of $4 \times CO_2$ coupled model with STC. Averages for the $2 \times CO_2$ and $4 \times CO_2$ are computed from their equilibrium climatologies

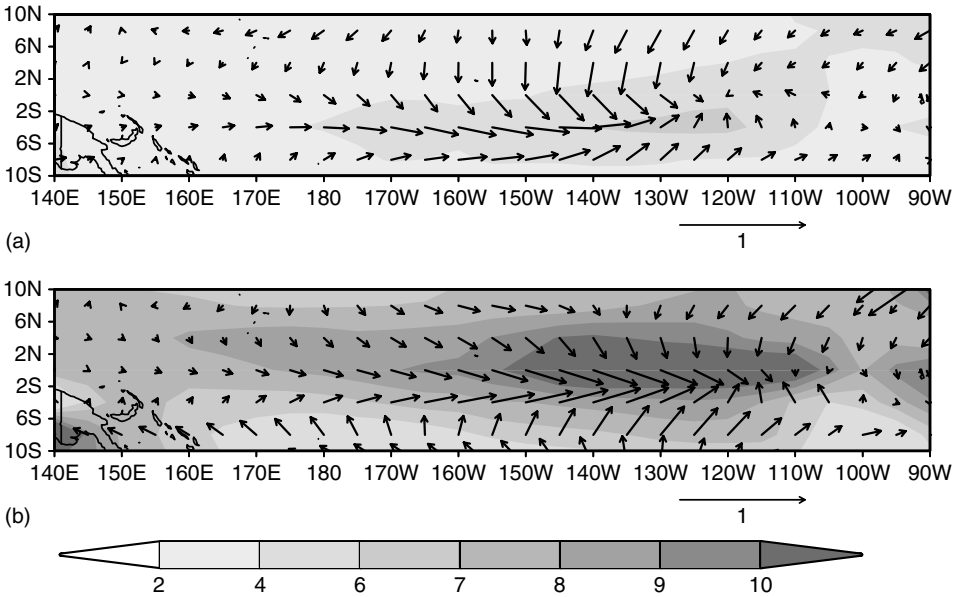

Figure 16. Mean DJF difference of SST (shaded, °C) and wind stress (vector, dyne/cm^2) for (a) of $2 \times CO_2$ coupled model simulation with STC – $1 \times CO_2$ coupled model simulation and (b) $4 \times CO_2$ coupled model simulation with STC – $1 \times CO_2$ coupled model simulation. Averages for the $2 \times CO_2$ and $4 \times CO_2$ simulations are computed from their equilibrium climatologies

being approximately 1.8 °C warmer for the experiment with the STC relative to the experiment without the STC. This agrees with Meehl *et al.* (2000) who produced a similar response using the NCAR CSM coupled model. Since El Niño induces global warming, it is not surprising that an El Niño-like response gives this result.

8. GLOBAL IMPLICATIONS OF AN EL NIÑO-LIKE RESPONSE

Because ENSO has fairly predictable effects on global weather patterns, it would be interesting to examine what impact a climatological redistribution of heat in the equatorial Pacific would have on the mean global weather. Since SST changes in the equatorial Pacific have the largest impact on global weather during the Northern Hemisphere winter, the results given in this section are for December–February (DJF). Given that three global-warming scenarios were run, i.e. q-flux, coupling without STC, and coupling with STC, it is logical to explore the effects of a quadruped CO_2 mean climate for three scenarios; (a) a q-flux climate, (b) a coupled climate with no effects from the STC, and (c) the effects of adding the STC to the coupled $4 \times CO_2$ climate. This approach allows the separation of radiative from dynamical effects. Scenario '(a)' is computed by subtracting the mean $4 \times CO_2$ winter q-flux climatology from the $1 \times CO_2$ q-flux climatology and addresses the radiative effects of increased CO_2 on a climate system containing a nondynamical ocean. Scenario '(b)' is computed by subtracting the mean $4 \times CO_2$ winter coupled climatology without the effects of the STC from the $1 \times CO_2$ coupled climatology and addresses the radiative effects of increased CO_2 on a coupled climate system which allows for a dynamical ocean in the tropical Pacific because of the inclusion of the ZC model. Finally, scenario '(c)' is computed by subtracting the mean $4 \times CO_2$ winter coupled climatology with the effects of the STC from the $4 \times CO_2$ coupled climatology without the effects of the STC, and addresses the dynamical effects of adding the STC to a $4 \times CO_2$ mean winter climate. Figures 20–24 describe the above scenarios for the SAT, 500 hPa height, 200 hPa wind, sea-level pressure (SLP), and precipitation for scenarios '(a)', '(b)', and '(c)'. For the SAT, (Figure 20), scenarios '(a)' and '(b)' are similar with general warming, with the greatest warming occurring over the high northern latitudes; scenario '(c)' shows the dynamical response to the El Niño-like climatology with warming that is especially

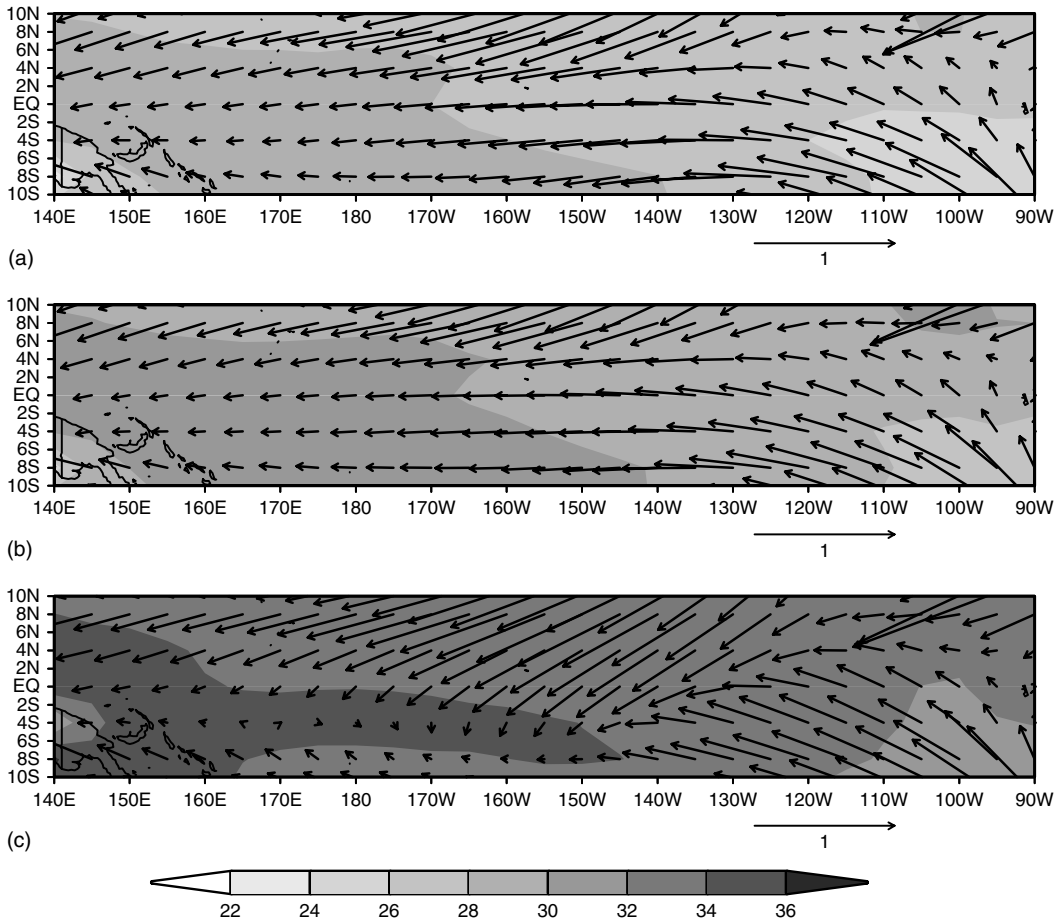

Figure 17. Mean DJF sea-surface temperature (shaded, °C) and wind stress (vector, dyne/cm^2) for (a) 50 year Mean annual average of $1 \times CO_2$ coupled model; (b) Year 90–140 average of $2 \times CO_2$ coupled model simulation without STC; (c) Year 160–210 average of $4 \times CO_2$ coupled model simulation without STC. Averages for the $2 \times CO_2$ and $4 \times CO_2$ simulations are computed from their equilibrium climatologies

prominent near the equator; other prominent areas in Figure 20(c) are over Africa and the northwestern Atlantic. For 500 hPa heights (Figure 21), scenario '(a)' shows a zonally symmetric pattern to height increases with heights increasing most at high latitudes relative to the tropics while the heights increase more or less uniformly independent of latitude in scenario '(b)'. Scenario '(c)' has the greatest height increases over the tropics consistent with an El Niño-like response; increases are also noted in the northwestern Atlantic. The 200 hPa wind differences (Figure 22) reveal some interesting behavior; scenarios (a) and (b) show negative 200 hPa wind anomalies (i.e. anomalous easterlies) in the equatorial Pacific with stronger winds indicating enhanced subtropical jet streams poleward of the negative anomaly. This pattern is consistent with what may be observed during an ENSO. Recall from Section 7 the discussion on how all of the global-warming scenarios reduced equatorial longitudinal SST gradients in the Pacific relative to their control runs; the 200 hPa wind response is likely a reflection of this effect; not surprisingly, for scenario (c) in which the longitudinal equatorial Pacific SST gradient is reversed, a similar but more intense 200 hPa wind structure occurs relative to scenarios (a) and (b). The SLP pattern (Figure 23) shows decreases in SLP over the eastern equatorial Pacific for scenarios (a) and (b) consistent with an atmospheric response to a reduced equatorial longitudinal SST gradient in the Pacific with additional reductions of SLP over Africa, the high northern polar latitudes, and in the midlatitudes in the South Pacific; increases in pressure are noted in a midlatitude zone extending from the North Pacific eastward across Europe; scenario (c) indicates the large differences that occur east of

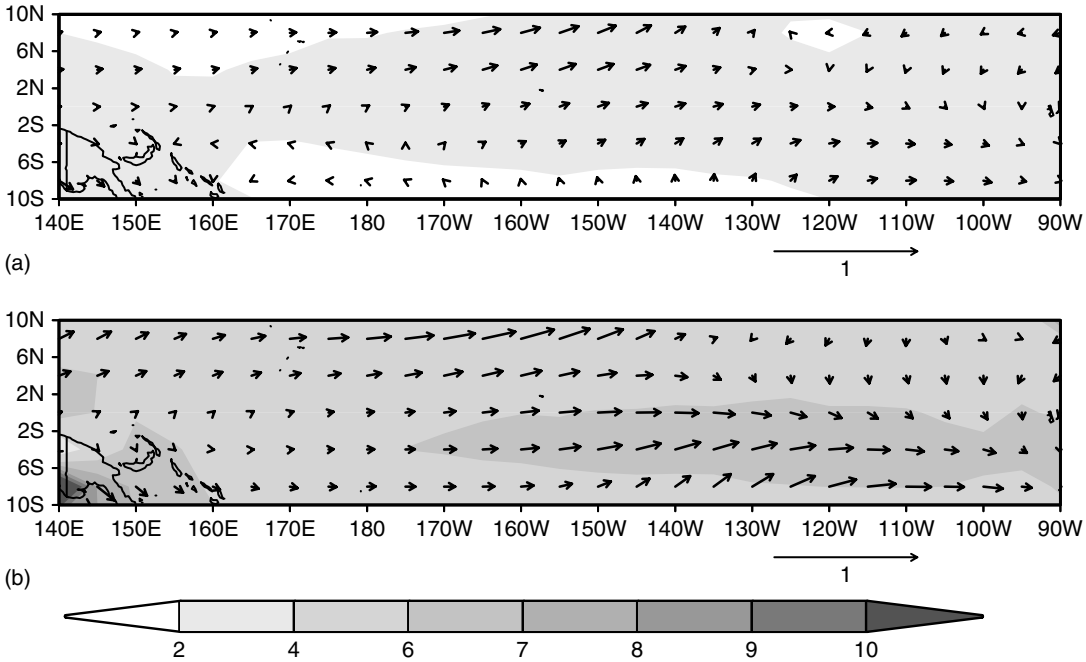

Figure 18. Mean DJF difference of SST (shaded, °C) and wind stress (vector, dyne/cm^2) for (a) $2 \times CO_2$ coupled model without STC – $1 \times CO_2$ coupled model and (b) $4 \times CO_2$ coupled model without STC – $1 \times CO_2$ coupled model. Averages for the $2 \times CO_2$ and $4 \times CO_2$ simulations are computed from their equilibrium climatologies

Australia (increase) and over the eastern Pacific (decrease), implying a negative southern oscillation index (SOI) due to the El Niño-like response. As in scenarios (a) and (b), scenario (c) produces a zone of increased SLP in midlatitudes from the North Pacific eastward to Europe; the similarity of the extratropical response for all of the scenarios may be because of the fact that all of the global-warming scenarios reduce the equatorial longitudinal SST gradient, with scenario (c) being best-defined in this regard. As with the other meteorological variables, scenarios (a) and (b) have similar precipitation differences (Figure 24); a double structure of increased precipitation is noted in the equatorial Pacific with one area near and just south of the equator and a second just north of the equator from the central Pacific into the Indian Ocean. Decreases are seen poleward of the first band in the east-central Pacific. Some less significant (though consistent) positive differences are located across the Aleutians, the central United States and near Iceland. Scenario (c) shows an enhanced zone of increased precipitation across the equatorial Pacific and to a somewhat lesser degree, across the Indian Ocean, with areas of compensatory decreases poleward of the increase in the Pacific; the tropical increases are in agreement with Meehl *et al.* (2000) who found similar increases. Areas of increased precipitation are also noted across the Aleutians, the eastern half of the United States, eastward across Europe, and the southern polar area.

From the above analysis, the effects of adding coupling to the AGCM is negligible in the global-warming response (i.e. comparing scenario (a) to scenario (b)); this is not surprising because the STC is inoperative in the first two scenarios. Although the radiative response to global warming does reduce the equatorial Pacific longitudinal SST gradient in both scenarios resulting in an El Niño-like response in their climatologies, the effect of adding the STC (i.e. scenario (c)) reduces (and even reverses) the equatorial Pacific longitudinal SST gradient, producing a much more intense El Niño-like atmospheric response relative to the other scenarios. The implication of these results is that any change to ENSO variability in a climatic sense, from radiative and especially from dynamical changes due to the STC, would have major impacts on global climate. Specifically, areas that are currently sensitive to the interannual effects of ENSO would have the potential for ENSO-related impacts to become part of their mean climatology, resulting in a more extreme climate.

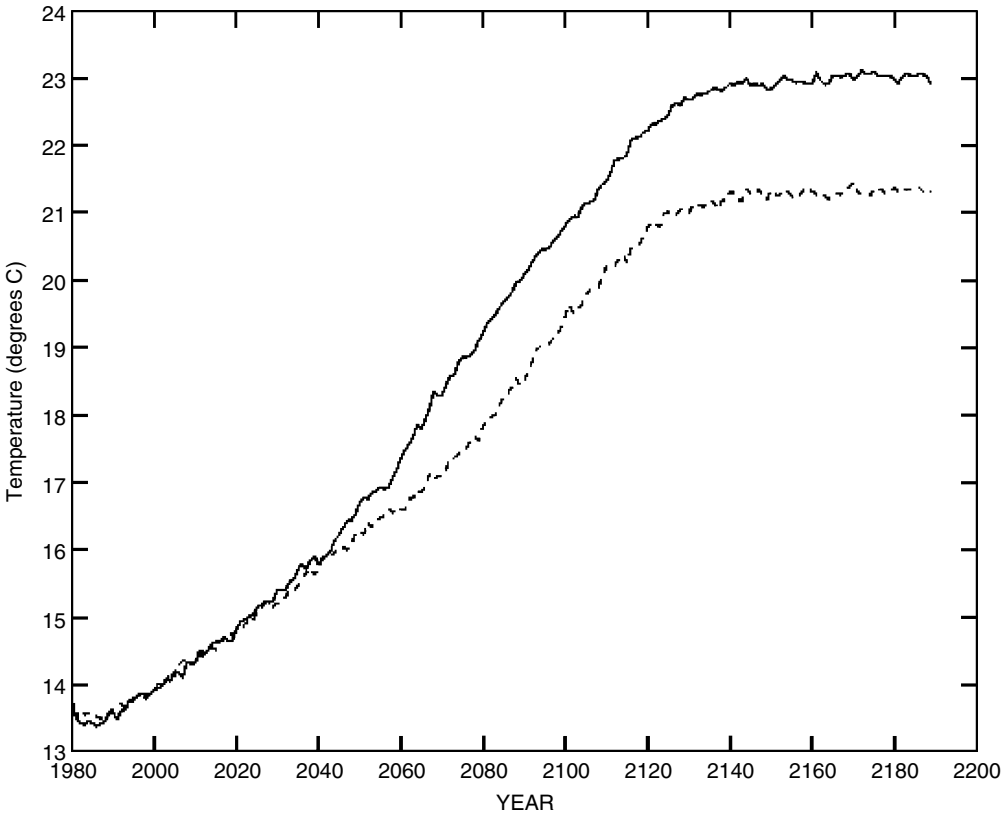

Figure 19. Time series of mean annual global SAT (°C), solid: $4 \times CO_2$ coupled model with STC dashed: $4 \times CO_2$ coupled model without STC

9. CONCLUSIONS

The GCM/ZC model is capable of producing an El Niño that is somewhat more frequent and lower in amplitude than the observed. This may be because of the weaker wind-stress anomalies produced by the GISS AGCM resulting in the reduction of the coupling strength. The GCM/ZC ENSO response exhibits a general westward propagation possibly due to wind-stress/SST interactions described in Battisti (1988). The GCM/ZC events appear to be locked into the annual cycle fairly similar to the observed annual cycle. In addition, the wind-stress anomalies produced represent an appropriate response to the SST anomalies (i.e. weaker trades associated with positive SST anomalies).

The GCM/ZC model's ENSO gives a realistic global atmospheric response, diagnosed by an increased PNA response in the 500 hPa height pattern, increased precipitation in the eastern Pacific and the southern United States, decreased precipitation in northeastern Brazil and the western Pacific, and increased 200 hPa winds associated with a stronger subtropical jet stream. The response, though spatially correct, is somewhat weaker than the observed, likely because of the relatively weak ENSO response in the GCM/ZC model; it is also possible that the GCM/ZC model physics (i.e. the AGCM's response to SST anomalies) may also play a role.

For global-warming induced ENSO change, the key mechanism controlling ENSO variability in the GCM/ZC model is the STC. In the simulations that include this mechanism, ENSO variability initially increases similar to the results obtained by Timmerman *et al*. (1999) and Collins (2000a). However, as the climate continues to become warm, so much heat is added to the equatorial-mixed layer that the longitudinal SST gradient in the equatorial Pacific is eliminated and an El Niño-like response occurs with small variability about this mean state. If the STC is not included, then there is a slight reduction in the longitudinal

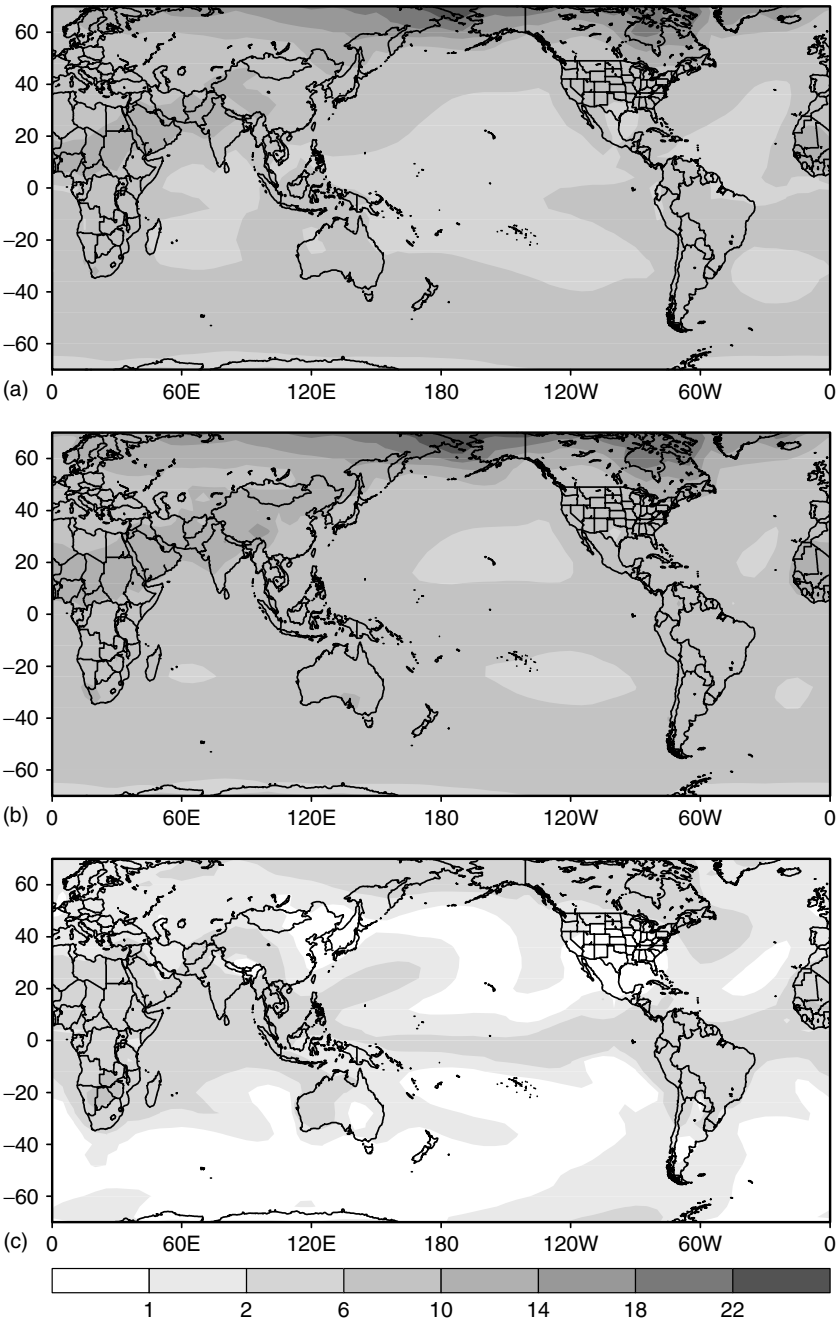

Figure 20. DJF SAT difference (°C) for (a) $4 \times CO_2$ q-flux simulation – $1 \times CO_2$ q-flux simulation; (b) $4 \times CO_2$ coupled model with no STC – $1 \times CO_2$ coupled model; (c) $4 \times CO_2$ coupled model with STC – $4 \times CO_2$ coupled model without STC. Averages for the $2 \times CO_2$ and $4 \times CO_2$ simulations are computed from their equilibrium climatologies

equatorial Pacific SST gradient, possibly due to cloud feedback as discussed by Meehl *et al*. (2000) or evaporative feedback as discussed by Knutson and Manabe (1995), Tett (1995), Knutson *et al*. (1997), Meehl and Washington (1996), Meehl and Washington (1986, 1989, 1996), Oglesby and Saltzman (1992), and Washington and Meehl (1993). Clouds can also operate as a negative feedback but may be overwhelmed by coupled dynamic feedbacks (Jin *et al*., 2001). Yu and Boer (2002) analyzed the Canadian Center for Climate

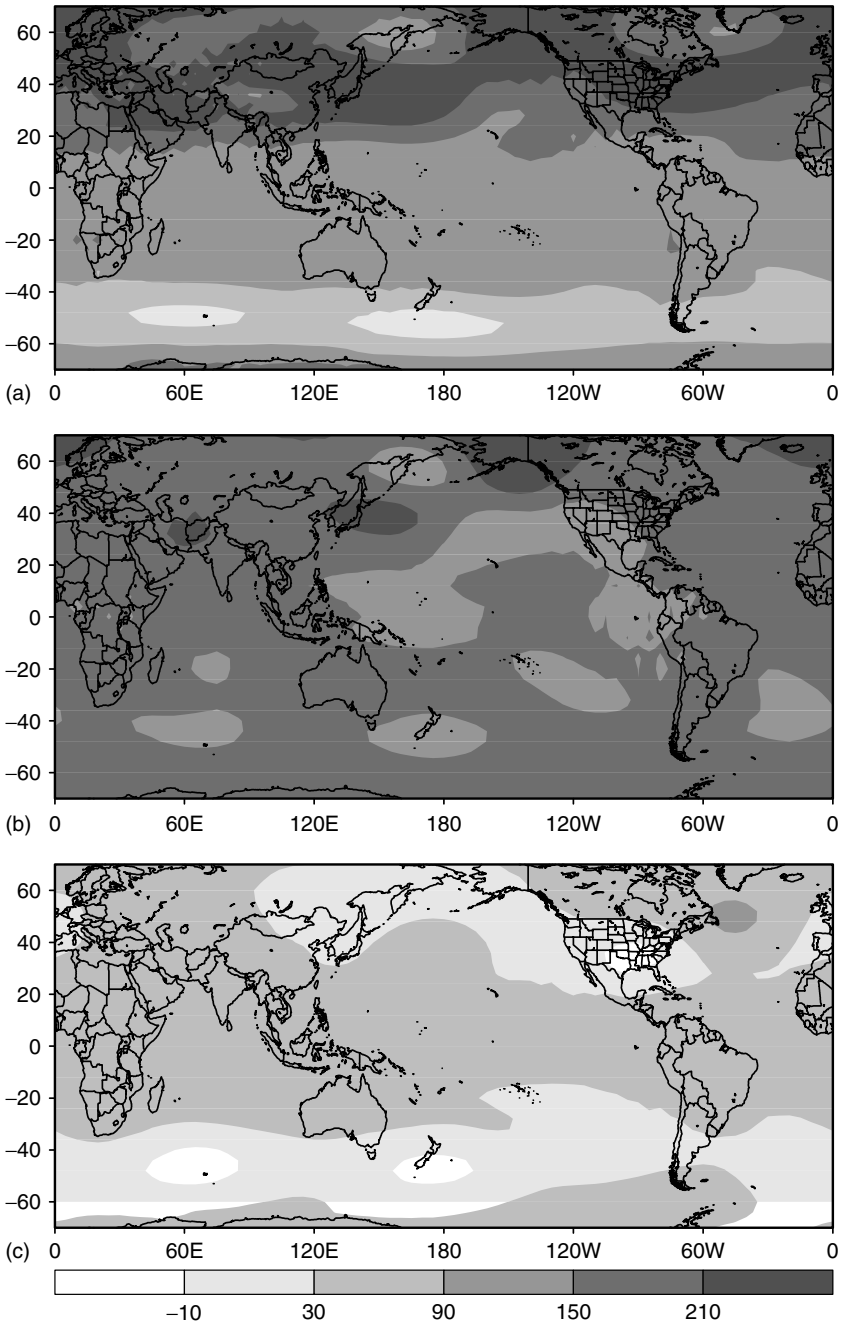

Figure 21. DJF 500 hPa height (m) for (a) $4 \times CO_2$ q-flux model – $1 \times CO_2$ q-flux model; (b) $4 \times CO_2$ coupled model with no STC – $1 \times CO_2$ coupled model; (c) $4 \times CO_2$ coupled model with STC – $4 \times CO_2$ coupled model without STC. Averages for the $2 \times CO_2$ and $4 \times CO_2$ simulations are computed from their equilibrium climatologies

Modeling and Analysis (CCCma) coupled GCM and concluded that negative cloud-radiative feedback does not preclude the existence of an El Niño-like response due to greenhouse forcing.

A feedback resulting from the El Niño-like response generated by including the STC is that global SAT increased to a higher equilibrium level relative to the CO_2 simulations not containing the STC (i.e. not containing the El Niño-like feature); so the El Niño-like feature impacts the magnitude of global warming.

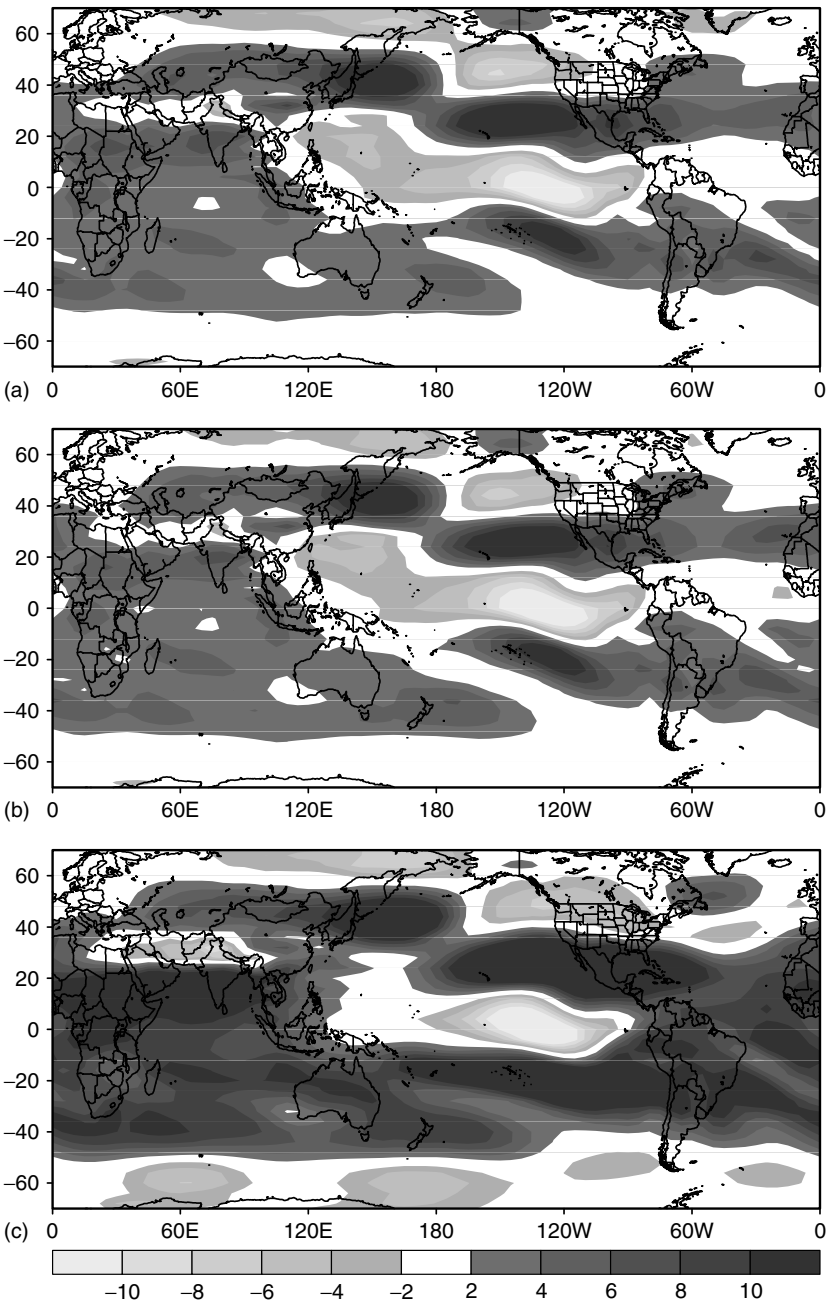

Figure 22. DJF 200 hPa wind (m/s) for (a) $4 \times CO_2$ q-flux model – $1 \times CO_2$ q-flux model; (b) $4 \times CO_2$ coupled model with no STC – $1 \times CO_2$ coupled model; (c) $4 \times CO_2$ coupled model with STC – $4 \times CO_2$ coupled model without STC. Averages for the $2 \times CO_2$ and $4 \times CO_2$ simulations are computed from their equilibrium climatologies

An analysis of the of mean winter precipitation, SAT, SLP, 500 hPa height, and 200 hPa winds shows an ENSO-like atmospheric response due to the radiative effects from increased CO_2 which results in a reduction of the equatorial Pacific longitudinal SST gradient. This effect is much more intense when adding the effects of the STC because the equatorial Pacific SST gradient is reduced and even reversed. Even if the STC depiction is too extreme, this paper demonstrates the potential implications on global climate due to changes in ENSO variability. As stated previously, the results given should be considered as that of a sensitivity study

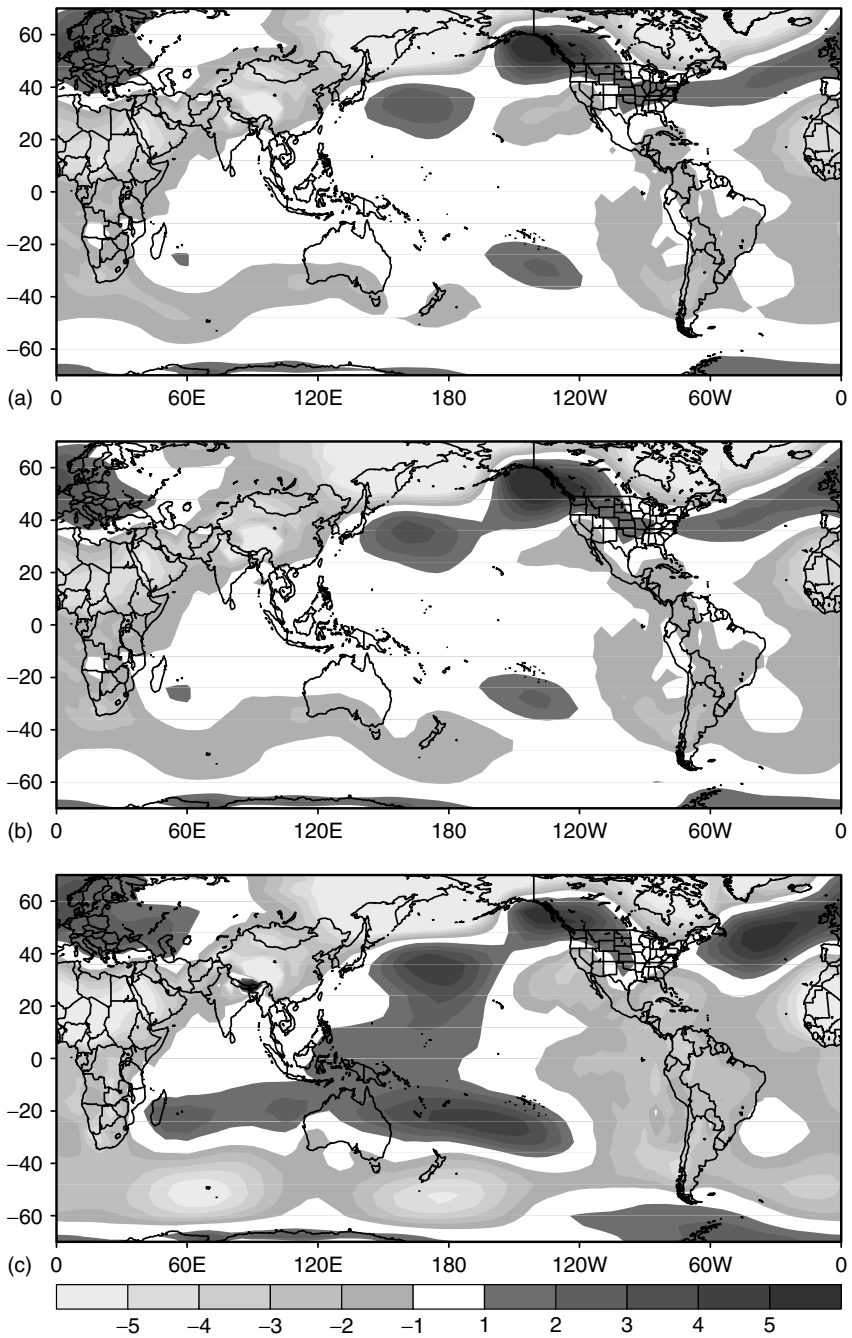

Figure 23. DJF SLP (mb) for (a) $4 \times CO_2$ q-flux model – $1 \times CO_2$ q-flux model; (b) $4 \times CO_2$ coupled model with no STC – $1 \times CO_2$ coupled model; (c) $4 \times CO_2$ coupled model with STC – $4 \times CO_2$ coupled model without STC. Averages for the $2 \times CO_2$ and $4 \times CO_2$ simulations are based on their equilibrium climatologies

exploring the physical impacts of inclusion of a STC of the strongest kind. However, the results outline the risk of having regional ENSO impacts transform from interannual variability into a part of the mean climate, resulting in a more extreme global climate. As understanding of the deep-ocean circulation improves, a more reliable estimate of the amount of heat carried by the STC will give more accurate assessments of its effects on ENSO and hence on global climate.

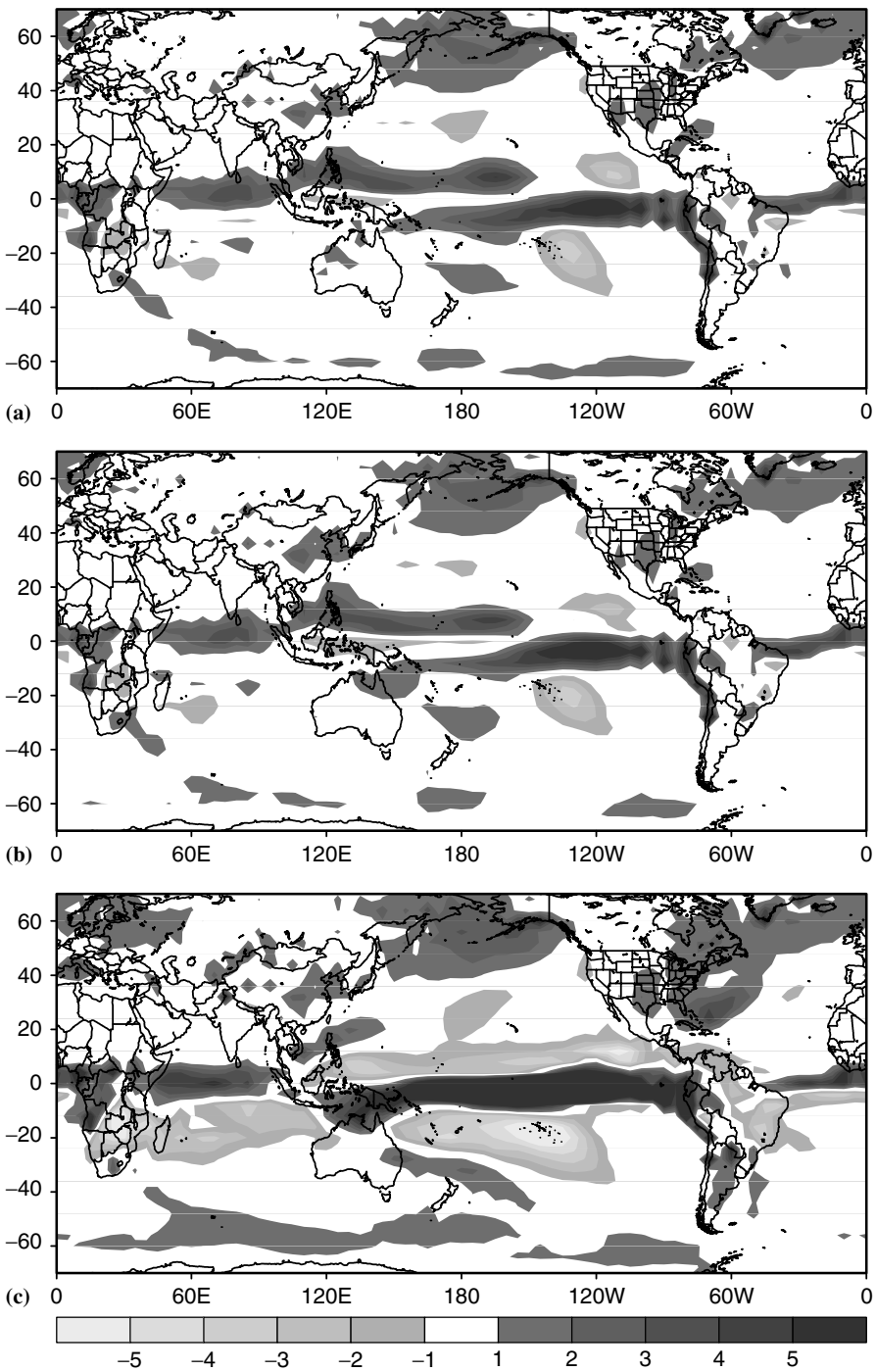

Figure 24. DJF precipitation (mm/day) for (a) $4 \times CO_2$ q-flux model – $1 \times CO_2$ q-flux model; (b) $4 \times CO_2$ coupled model with no STC – $1 \times CO_2$ coupled model; (c): $4 \times CO_2$ coupled model with STC – $4 \times CO_2$ coupled model without STC. Averages for the $2 \times CO_2$ and $4 \times CO_2$ simulations are computed from their equilibrium climatologies

APPENDIX I

The original GCM is coupled to a q-flux ocean, which allows the SST to change in response to changes in the surface heat balance defined as:

$$\partial_t T' = Q'/C_p \rho H \tag{1}$$

In Equation (1), ρ is density, T is sea-surface temperature anomaly, t is time, C_p is heat capacity at constant pressure, H is mixed layer depth, and Q' is surface heating anomaly. Changes in Q can further be defined as:

$$Q' = SH' + LH' + SW' + LW' \tag{2}$$

where SH' is the sensible heat anomaly, LH' is the latent heat anomaly, SW' is the shortwave radiation anomaly incident on the surface, and LW' is the long-wave radiation anomaly.

Since the q-flux model is incapable of generating ENSO, coupling the GCM to ZC offers a possible way for the GCM ocean to simulate ENSO. To accomplish this, the surface heating balance in the GCM's tropical Pacific was altered to include heating due to the wind-stress driven circulation field in the equatorial Pacific. The dynamical heat balance can be expressed using Equation (1) as:

$$Q'_{\mathrm{dyn}} = \partial_t T' C_p \rho H \tag{3}$$

where Q'_{dyn} is the dynamical heating tendency obtained from ZC due to wind-stress forcing from the GCM and $\partial_t T'$ is the SST change to dynamical effects in the ZC model. Now, this term is added to the GCM's surface heat balance so that:

$$Q' = SH' + LH' + SW' + LW' + Q'_{\mathrm{dyn}} \tag{4}$$

To generate the balance shown in Equation (4) in the GCM ocean, the GCM is run for 10 days (10 days because this is the timestep of ZC), which generates a 10 day mean wind-stress anomaly (anomaly taken from a monthly climatology of the original 50 year run of B178). The ZC ocean model is then run for 10 days using the GCM wind-stress anomaly to drive their ocean. The dynamical heating component from the 10-day run of ZC is then inserted into the GCM surface heat balance over the domain of ZC (i.e. 19 °N–19 °S 120 °E–70 °W) once per hour and the GCM is run for 10 days generating a 10-day wind-stress anomaly, which is used to drive the ZC model, and so on. This procedure is used to run the coupled GCM/ZC model for 50 years.

ACKNOWLEDGEMENTS

We gratefully acknowledge the assistance of Radley Horton and Angel Suarez of NASA/GISS for assistance with model data. We would also like to thank the three anonymous reviewers who helped to improve this manuscript.

REFERENCES

Bacher A, Oberhuber JM, Roeckner E. 1998. ENSO dynamics and seasonal cycle in the tropical Pacific as simulated by the ECHAM4/OPYC3 coupled general circulation model. *Climate Dynamics* **14**: 431–450.

Barnett TP, Pierce DW, Latif M, Dommenget D, Saravanan R. 1999. Interdecadal interactions between the tropics and midlatitudes in the Pacific basin. *Geophysical Research Letters* **26**: 615–618.

Battisti D. 1988. Dynamics and thermodynamics of a warming event in a coupled tropical atmosphere-ocean model. *Journal of the Atmospheric Sciences* **45**: 2889–2919.

Boer GJ, Yu B, Kim S-J, Flato GM. 2004. Is there observational support for an El Niño-like pattern of future global warming? *Geophysical Research Letters* **31**: L06201.

Cane MA, Zebiak SE, Dolan SC. 1986. Experimental forecasts of El Niño. *Nature* **321**: 827–832.

Cane MA, Clement AC, Kaplan A, Kushnir Y, Pozdnyakov D, Seager R, Zebiak S. 1997. Twentieth century sea surface temperature trends. *Science* **275**: 957–960.
Clement AC, Seager RS, Cane MA, Zebiak SE. 1996. An ocean dynamical thermostat. *Journal of Climate* **9**: 2190–2193.
Collins M. 2000a. The El Niño-Southern oscillation in the second Hadley centre coupled model and its response to greenhouse warming. *Journal of Climate* **13**: 1299–1312.
Collins M. 2000b. Understanding uncertainties in the response of ENSO to greenhouse warming. *Geophysical Research Letters* **27**: 3509–3512.
Collins M. the CMIP Modeling Groups. 2005. El Niño- or La Niña-like climate change? *Climate Dynamics* **24**: 89–104.
Fine RA, Peterson WH, Ostlund HG. 1987. The penetration of Tritium into the tropical Pacific. *Journal of Physical Oceanography* **17**: 553–564.
Gu D, Philander SGH. 1997. Interdecadal climate fluctuations that depend on exchanges between the tropics and the extratropics. *Science* **275**: 805–807.
Guilyardi E. 2005. El Niño-mean state-seasonal cycle interactions in a multi-model ensemble. *Climate Dynamics* Published online, DOI:10.1007/s00382-005-0084-6.
Hansen J, Fung J, Lacis A, Rind D, Lebedeff S, Ruedy R, Russell G, Stone P. 1988. Global climate changes as forecast by Goddard institute for space studies three-dimensional model. *Journal of Geophysical Research* **93**: 9341–9364.
Hartke G, Rind D. 1997. Improved surface and boundary layer models for the Goddard institute for space studies general circulation model. *Journal of Geophysical Research* **102**: 16407–16422.
Jin F-F, Hu Z-Z, Latif M, Bengtsson L, Roeckner E. 2001. Dynamical and cloud-radiation feedbacks in El Niño and greenhouse warming. *Journal of Geophysical Research* **28**: 1539–1542.
Kaplan A, Cane M, Kushnir Y, Clement A, Blumenthal B, Rajagopalan B. 1998. Analyses of global sea surface temperatures 1856–1991. *Journal of Geophysical Research* **103**: 18567–18589.
Kleeman R, McCreary JP, Klinger B. 1999. A mechanism for generating ENSO decadal variability. *Geophysical Research Letters* **26**: 1743–1746.
Knutson TR, Manabe S. 1995. Time-mean response over the Tropical Pacific to increased CO_2 in a coupled ocean-atmosphere model. *Journal of Climate* **8**: 2181–2199.
Knutson TR, Manabe S, Gu D. 1997. Simulated ENSO in a global coupled ocean-atmosphere model: multidecadal amplitude modulation and CO_2 sensitivity. *Journal of Climate* **10**: 138–161.
Kumar A, Hoerling M. 1997. Interpretation and implications of the observed inter-El Niño variability. *Journal of Climate* **10**: 83–91.
Latif M, Anderson D, Barnett T, Cane M, Kleeman R, Leetma A, O'Brien J, Rosati A, Schneider E. 1998. A review of the predictability and prediction of ENSO. *Journal of Geophysical Research* **103**: 14 375–14 393.
Latif M, Kleeman R, Eckert C. 1997. Greenhouse warming, decadal variability, or El Niño? An attempt to understand the anomalous 1990s. *Journal of Climate* **10**: 2221–2238.
Lee T, Fukumori I. 2003. Interannual-to-decadal variations of tropical-subtropical exchange in the Pacific ocean: Boundary versus interior pycnocline transports. *Journal of Climate* **16**: 4022–4042.
Liu Z. 1994. A simple model of the mass exchange between the subtropical and Tropical Ocean. *Journal of Physical Oceanography* **24**: 1153–1165.
Liu Z. 1998. The role of ocean in the response of tropical climatology to global warming: The east-west contrast. *Journal of Climate* **11**: 864–875.
Liu Z, Huang B. 1998. Why is there a tritium maximum in the central equatorial Pacific thermocline? *Journal of Physical Oceanography* **28**: 1527–1533.
Liu Z, Shin S-I. 1999. On thermal ventilation of active and passive tracers. *Geophysical Research Letters* **26**: 357–360.
Lu P, McCreary JP. 1995. Influence of the ITCZ on the flow of thermocline water from the subtropical to the equatorial ocean. *Journal of Physical Oceanography* **25**: 3076–3088.
McCreary JP Jr, Anderson DLT. 1991. An overview of coupled ocean-atmosphere models of El Niño and the Southern oscillation. *Journal of Geophysical Research* **96**: 3125–3150.
McCreary JP, Lu P. 1994. Interaction between the subtropical and equatorial ocean circulations: the subtropical cell. *Journal of Physical Oceanography* **24**: 66–497.
McPhaden MJ, Zhang D. 2002. Slowdown of the meridional overturning circulation in the upper Pacific ocean. *Nature* **415**: 603–608.
Meehl GA, Washington WM. 1986. Tropical response to increased CO_2 in a GCM with a simple mixed-layer ocean: similarities to an observed Pacific warm event. *Monthly Weather Review* **114**: 667–674.
Meehl GA, Washington WM. 1989. Climate sensitivity due to increased CO_2: Experiments with a coupled atmosphere and ocean general circulation model. *Climate Dynamics* **4**: 1–38.
Meehl GA, Washington WM. 1996. El Niño-Like climate change in a model with increased atmospheric CO_2 concentrations. *Nature* **382**: 56–60.
Meehl GA, Arblaster J. 1998. The Asian-Australian monsoon and El Niño-Southern oscillation in the NCAR climate system model. *Journal of Climate* **11**: 1356–1385.
Meehl GA, Collins WD, Boville BA, Kielhl JT, Wigley TML, Arblaster J. 2000. Response of the NCAR climate system model to increased CO_2 and the role of physical processes. *Journal of Climate* **13**: 1879–1898.
Meehl GA, Gent PR, Arblaster JM, Otto-Bliesner BL, Brady EC, Craig A. 2001. Factors that affect the amplitude of El Niño in global coupled climate models. *Climate Dynamics* **17**: 515–526.
Meehl GA, Teng H, Branstator GW. 2005. Future changes of El Niño in two global coupled climate models. *Climate Dynamics* submitted.
Merryfield W. 2005. Changes to ENSO under CO_2 doubling in the IPCC AR4 coupled climate models. *Journal of Climate* submitted.
Murtugudde R, Seager R, Busalacchi AJ. 1996. Simulation of the tropical oceans with an ocean GCM coupled to an atmospheric mixed-layer model. *Journal of Climate* **9**: 1795–1815.
Neelin JD, Battisti D, Hirst A, Jin F, Wakata Y, Yamagata T, Zebiak S. 1998. ENSO theory. *Journal of Geophysical Research* **103**: 14261–14290.

Neelin JD, Latif M, Allaart MAF, Cane MA, Cubasch U, Gates WL, Gent PR, Ghil M, Gordon C, Lau NC, Mechoso CR, Meehl GA, Oberhuber JM, Philander SGH, Schopf PS, Sperber KR, Sterl A, Tokioka T, Tribbia J, Zebiak SE. 1992. Tropical air-sea interaction in general circulation models. *Climate Dynamics* **7**: 73–104.

Nonaka M, Xie SP, Takeuchi K. 2000. Equatorward spreading of a passive tracer with application to North Pacific interdecadal temperature variations. *Journal of Oceanography* **56**: 173–183.

Oglesby RJ, Saltzman B. 1992. Equilibrium climate statistics of a general circulation model as a function of atmospheric carbon dioxide. Part I: geographic distributions of primary variables. *Journal of Climate* **5**: 66–92.

Rasmusson EM, Carpenter TH. 1982. Variations in tropical sea surface temperatures and surface wind fields associated with the Southern oscillation/El Niño. *Monthly Weather Review* **110**: 354–384.

Seager R, Kushnir Y, Cane MA. 1995. On heat flux boundary conditions for ocean models. *Journal of Physical Oceanography* **25**: 3219–3230.

Seager R, Murtugudde R. 1997. Ocean dynamics, thermocline adjustment, and regulation of tropical SST. *Journal of Climate* **10**: 521–534.

Schneider N, Venzke S, Miller AJ, Pierce DW, Barnett TP, Deser C, Latif M. 1999. Pacific thermocline bridge revisited. *Geophysical Research Letters* **26**: 1329–1332.

Tett S. 1995. Simulation of El Niño-Southern oscillation-like variability in a global AOGCM and its response to CO_2 increase. *Journal of Climate* **8**: 1473–1502.

Timmerman A, Oberhuber J, Bacher A, Esch M, Latif M, Roeckner E. 1999. Increased El Niño frequency in a climate model forced by future greenhouse warming. *Nature* **398**: 694–696.

Trenberth KE, Branstator GW, Karoly D, Kumar A, Lau N-C, Ropelewski C. 1998. Progress during TOGA in understanding and modeling global teleconnections associated with tropical sea surface temperatures. *Journal of Geophysical Research* **103**: 14291–14324.

Washington WM, Meehl GA. 1993. Greenhouse sensitivity experiments with penetrative cumulus convection and tropical cirrus albedo effects. *Climate Dynamics* **8**: 211–223.

Wong APS, Johnson G. 2003. South Pacific eastern subtropical mode water. *Journal of Physical Oceanography* **33**: 1493–1509.

Yu B, Boer GJ. 2002. The roles of radiation and dynamical processes in the El Niño-like response to global warming. *Climate Dynamics* **19**: 539–553.

Zebiak SE, Cane M. 1987. A model ENSO. *Monthly Weather Review* **115**: 2262–2278.

http://www.cpc.ncep.noaa.gov/data/indices/sstoi.indices (Monthly El Niño Indices) from the Climate Prediction Center (1950-Present).

